Autophagy 11:7, 1081–1098; July 2015; Published with license by Taylor & Francis Group, LLC

MYBL2 guides autophagy suppressor VDAC2 in the developing ovary to inhibit autophagy through a complex of VDAC2-BECN1-BCL2L1 in mammals

Jia Yuan, Ying Zhang, Yue Sheng, Xiazhou Fu, Hanhua Cheng,* Rongjia Zhou*

Department of Genetics; College of Life Sciences; Wuhan University; Wuhan, China

Keywords: Beclin1, MYBL2, ovary, reproduction, transcription regulation, VDAC2

Abbreviations: ATG5, autophagy-related 5; ATG12, autophagy-related 12; ATG16L1, autophagy-related 16-like 1; BAK, BCL2-antagonist/killer 1; BCL2, B-cell CLL/lymphoma 2; BCL2L1, BCL2-like 1; BECN1, Beclin 1, autophagy related; CDS, coding DNA sequence; Dpp, days postpartum; GATA1, GATA binding protein 1 (globin transcription factor 1); GATA2, GATA binding protein 2; LC3B, microtubule-associated protein 1 light chain 3 beta; MBS, MYBL2 binding site; MYBL2, v-myb avian myeloblastosis viral oncogene homolog-like 2; SP1, Sp1 transcription factor; VDAC, voltage-dependent anion channel; wt, wild type.

Oogenesis is essential for female gamete production in mammals. The total number of ovarian follicles is determined early in life and production of ovarian oocytes is thought to stop during the lifetime. However, the molecular mechanisms underling oogenesis, particularly autophagy regulation in the ovary, remain largely unknown. Here, we reveal an important MYBL2-VDAC2-BECN1-BCL2L1 pathway linking autophagy suppression in the developing ovary. The transcription factors GATA1 and MYBL2 can bind to and activate the *Vdac2* promoter. MYBL2 regulates the spatiotemporal expression of VDAC2 in the developing ovary. Strikingly, in the *VDAC2* transgenic pigs (*Sus scrofa*/Ss), VDAC2 exerts its function by inhibiting autophagy in the ovary. In contrast, *Vdac2* knockout promotes autophagy. Moreover, VDAC2-mediated autophagy suppression is dependent on its interactions with both BECN1 and BCL2L1 to stabilize the BECN1 and BCL2L1 complex, suggesting VDAC2 as an autophagy suppressor in the pathway. Our findings provide a functional connection among the VDAC2, MYBL2, the BECN1-BCL2L1 pathway and autophagy suppression in the developing ovary, which is implicated in improving female fecundity.

Introduction

In the mammalian ovary, folliculogenesis begins from primordial germ cells, proceeds through the primary follicle stage to the mature follicle stage and finally produces functional oocytes. The total number of ovarian follicles is determined early in life and production of ovarian oocytes is thought to stop later in life. Thus, ovarian senescence probably attributes to the exhaustion of reserved primordial follicles. Meanwhile, atresia occurs in many early follicles to ensure the growth of dominant follicles, thus a few oocytes develop to maturation. Follicles, which are functional units of the ovary, support oocyte growth and development. Somatic granulosa cells and cumulus cells surround oocytes, and their interactions are important for oogenesis.[1-5] Granulosa cell apoptosis may occur in the inner surface of the granulosa layers and then may extend to the outer layers near the follicular theca,[6] which might aid follicular atresia. Granulosa cells can provide several factors, such as specific amino acids and cholesterol, to metabolic pathways in oocytes;[5] however, oocytes can regulate gene expression in granulosa cells through oocyte-derived paracrine factors, including GDF9 (growth differentiation factor 9) and BMP15 (bone morphogenetic protein 15).[5,7] The interaction between oocytes and granulosa cells seems important for oogenesis. However, the molecular mechanisms of folliculogenesis are not completely understood yet. Identification of the key molecular events that control follicular development will help us to understand ovarian functions.

Oogenesis is a complicated process during which the balance between pro- and anti-apoptosis factors is pivotal for accurately

*Correspondence to: Rongjia Zhou; Email: rjzhou@whu.edu.cn, Hanhua Cheng; Email: hhcheng@whu.edu.cn
Submitted: 08/12/2014; Revised: 03/30/2015; Accepted: 04/09/2015
http://dx.doi.org/10.1080/15548627.2015.1040970

regulating follicular atresia and dominant follicle development. BCL2 family members are important regulators of apoptosis during mammalian ovary development.[8-12] Several members of this family, including BCL2L1 and BCL2, are also involved in autophagy regulation.[13,14] Nutrient deprivation may induce autophagy during the germarium and mid-oogenesis stages of the *Drosophila* ovary to significantly decrease egg production.[15-17] The phenotype of autophagy-deficient stroma follicle cells in *Drosophila* exhibits multiple egg chamber defects.[18] Increasing evidence has indicated that follicular atresia is associated with autophagy regulation in mammals. Dying oocytes in the developing rat ovary can activate both an apoptosis regulator, CASP3 (caspase 3, apoptosis-related cysteine peptidase), and an autophagy marker, LAMP1 (lysosomal-associated membrane protein 1).[19] Autophagy may occur in granulosa cells and oocytes, which is associated with apoptosis.[19,20] In addition, cigarette smoke exposure may promote autophagy of granulosa cells in mice.[21] These data suggest that autophagy may occur in female germ cells. However, the molecular mechanisms connecting autophagy and ovarian functions remain largely unknown.

The VDAC (voltage-dependent anion channel) family comprises 3 members: VDAC1, 2, and 3. VDAC2 is a mitochondrial outer-membrane channel protein that plays pivotal roles in apoptosis together with several members of the BCL2 family, such as BCL2L1 and BAK1 (BCL2-antagonist/killer 1).[22-27] VDAC2 directly interacts with BAK1 to inhibit its oligomerization, thus suppressing cell apoptosis.[22] A VDAC2 defect in thymocytes can cause apoptosis.[25] VDAC2 also has a direct interaction with BCL2L1, and VDAC2 overexpression can effectively inhibit BCL2L1-induced apoptosis.[24] In addition, another BCL2 family member, truncated BID/tBID (truncated BH3 interacting domain death agonist), can regulate apoptosis through VDAC2.[26] *Vdac3* (voltage-dependent anion channel 3)-deficient male mice are healthy but infertile because of a structural abnormality of sperm.[28] VDAC1 (voltage-dependent anion channel 1) interacts with BAX (BCL2-associated × protein), BCL2L1 and BCL2 and regulates apoptosis.[29,30] A recent study demonstrates that VDAC1 (voltage-dependent anion channel 1) is involved in PINK1/Parkin-mediated mitophagy.[31] Whether VDAC2 is involved in autophagy, particularly in the ovary, remains unknown. Our recent study in pigs (Ss) demonstrates that SsVDAC2 is upregulated in the ovary by long-term litter size selection,[32] hinting at a role for SsVDAC2 in ovarian functions.

In this report, we identified regulatory elements of *Vdac2* expression in the developing ovary. Both in vitro and in vivo analyses demonstrated that transcription factors GATA1 and MYBL2 could bind to and activate the *Vdac2* promoter. Transgenic and knockout analyses revealed that VDAC2 exerts its function by inhibiting autophagy. Furthermore, we demonstrated that VDAC2 inhibits autophagy by interacting with BECN1 and BCL2L1 to stabilize the BECN1 and BCL2L1 complex. Our research provides the basis for VDAC2 participation in follicular development through autophagy suppression in mammals, highlighting an importance of autophagy suppression during oogenesis in mammals.

Results

Identification of regulatory elements of *Vdac2* expression in the ovary

To explore the *Vdac2* expression pattern in the developing ovary, real-time quantitative PCR was first used to analyze *Vdac2* mRNA expression during ovary development in postnatal mice. The RT-PCR results showed that *Vdac2* mRNA expression increased to 14 d postpartum (dpp) and then gradually decreased to a stable level that remained until adulthood (**Fig. 1A**). Western blot analyses confirmed this expression trend at the protein level (**Fig. 1B**). Furthermore, immunofluorescence indicated that VDAC2 was expressed in the cytoplasm of stromal cells and in the primordial germ cells at 2 dpp. Along with primary follicle development at 6 dpp, VDAC2 was expressed in the granulosa cells, oocytes and basement membranes, whereas VDAC2 expression in oocytes was markedly increased, with a high level remaining until adulthood. In the granulosa cells, VDAC2 peak expression was observed at 14 dpp, with a high level remaining until adulthood, where its expression decreased in theca cells after 14 dpp (**Fig. 1C** and **S1**). These results indicate that VDAC2 is likely to be involved in follicle development.

To identify the regulatory elements of *Vdac2* expression in the ovary, a series of deletions of the *Vdac2* potential promoter were used to drive luciferase gene expression and luciferase activity was determined. The results showed that the sequence from −339 bp to −272 bp in the 5' flanking region is key for *Vdac2* transcriptional activity (**Fig. 2A and B**). The core promoter region was in a CpG island but lacked a TATA box. The methylation analysis showed that the CpG island was unmethylated in the ovary from 2 dpp to adulthood (**Fig. S2**). Because this promoter is open and active in the developing ovary, TFSEARCH software was used to determine the potential transcription factor binding sites, which were further confirmed by mutation analysis. A GC box (−337 bp to −327 bp), a GATA-like element (−307 bp to −296 bp) and 2 MYBL2 binding sites (MBS) (−286 bp to −260 bp) were detected in the promoter region (**Fig. 2A**). To identify the roles of these sites, site-directed mutants were constructed using wild-type pGL3-LS7 plasmid as the template. Compared with the wild-type pGL3-LS7 construct, the double MBS mutants and GC box mutant showed an obvious decrease in promoter activity, with particularly low activity observed in the GATA-like element mutant (**Fig. 2C**). However, the single MBS mutant showed the same transcription activity as the wild type. As parallel controls, the same site-directed mutagenesis was used, with the wild-type pGL3-LS1 plasmid as the template, and the results were similar to the pGL3-LS7 mutagenesis (**Fig. S3**). These results indicate that the binding sites for the transcription factors GATA and MYB are important for *Vdac2* promoter activity.

GATA1 and MYBL2 activate the *Vdac2* promoter

A luciferase reporter analysis was used to determine the binding of the transcription factors GATA, MYB, and SP1 to the GATA-like element, MBS and the GC box, respectively. The analysis showed that SP1 has no effect on the luciferase activity

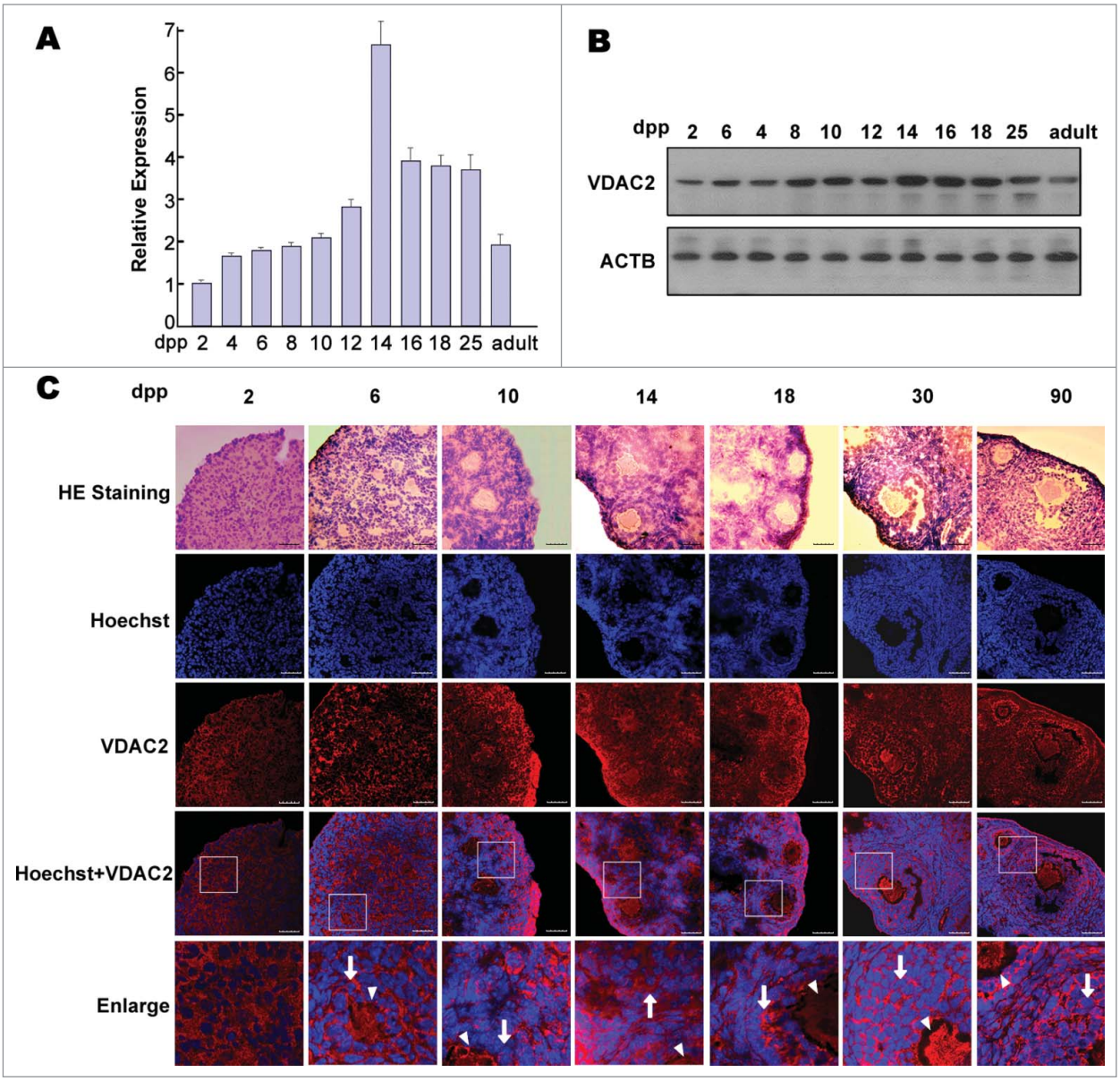

Figure 1. *Vdac2* expression in the developing ovaries of postnatal mice. (**A**) Real-time quantitative RT-PCR indicates that *Vdac2* is expressed in postnatal and adult ovaries, with a peak at 14dpp. *Actb* was used as an internal control. (**B**) Western blot analysis shows VDAC2 expression in postnatal and adult ovaries, with a peak at 16 dpp. ACTB was used as a control. (**C**) Immunofluorescence of the VDAC2 protein in the developing ovaries of postnatal mice using the anti-VDAC2 antibody. VDAC2 is expressed in the cytoplasm of stromal cells and oocytes at 2 dpp; VDAC2 expression gradually increases from 6 dpp to 18 dpp in oocytes, theca and granulosa cells. After 18 dpp, VDAC2 maintains high expression in oocytes and granulosa cells but less in theca cells. HE staining indicates the ovary tissue structure. The nuclei were stained by Hoechst. The enlarged images originated from the regions with white squares. The arrows indicate granulosa cells, and arrowheads show the oocytes. Scale bar: 50 μm. See also **Figure S1**.

(**Fig. 3A and B**). Additionally, GATA1, but not GATA2, could significantly increase *Vdac2*-LS7-driven luciferase activity. By contrast, the activity of the GATA-like element site mutant was not upregulated by GATA1. GATA1 cotransfection with GATA2 also had no contribution to the GATA1 activity (**Fig. 3A and C**). Moreover, mutations in the 20 bp sequence between the GC-box and GATA-like element decreased the *Vdac2* promoter activity, and the mutation closer to the GATA-like element had lower activity (**Fig. 3A and D**). These results show that the GATA-like element and its 30 bp upstream region, including the GC box, are key regions for GATA1 binding. MYBL2 transfection upregulated the *Vdac2*-LS7-driven or single MBS mutation-driven luciferase activity, whereas MYBL2 had no effect on the promoter activity of the double-MBS site mutant (**Fig. 3A and E**), suggesting that MYBL2 can bind to both MBS sites in the *Vdac2* promoter and activate the promoter activity. In addition, endogenous *Vdac2* could also be upregulated by overexpression of GATA1 and MYBL2 in both CHO and NIH-3T3

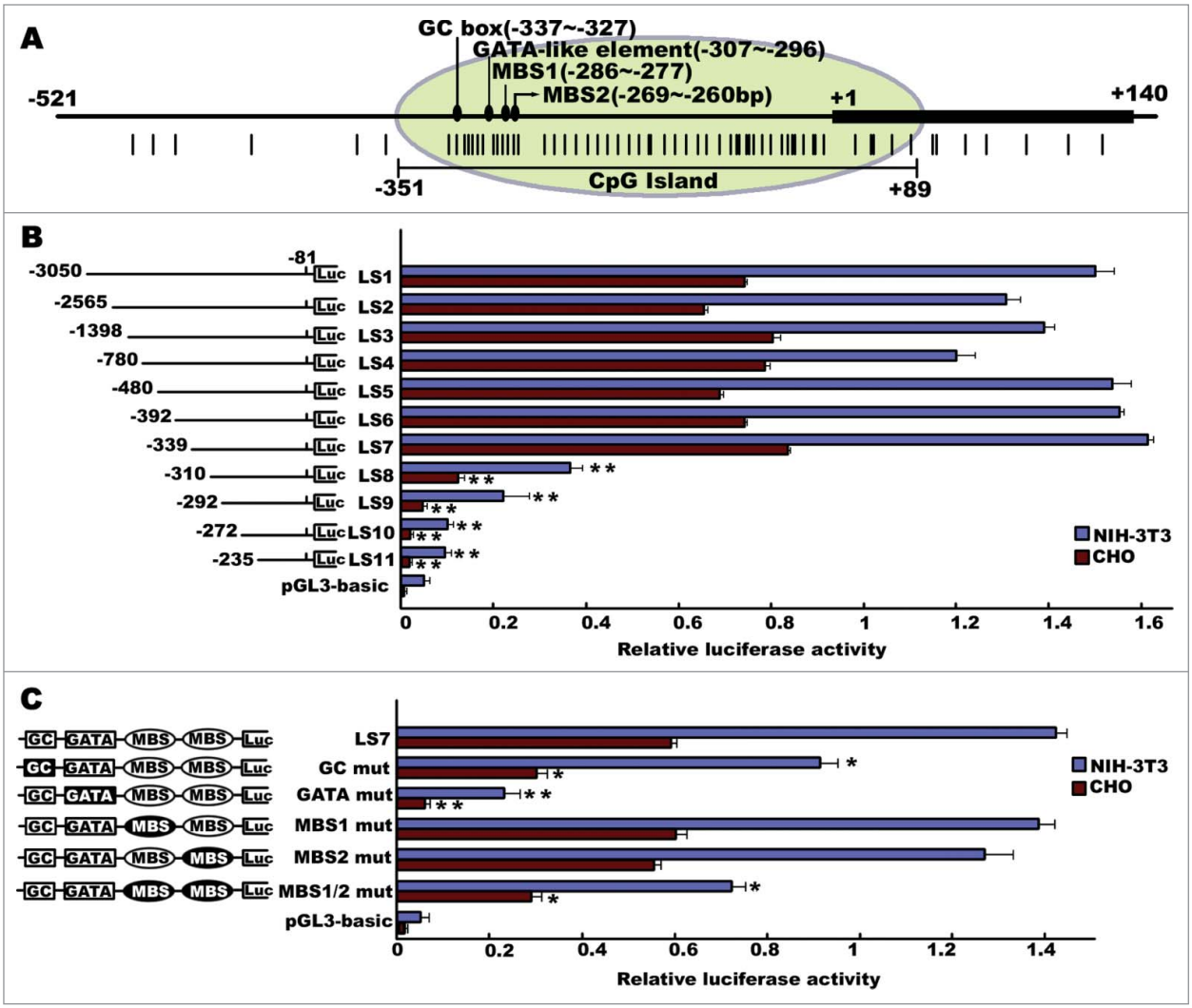

Figure 2. Mutation analysis of the mouse *Vdac2* promoter. (**A**) Schematic diagram of the *Vdac2* promoter, which includes a CpG island with a GC box, a GATA-like element and 2 MBS sites. The short vertical bars indicate CpG dinucleotides. (**B**) Luciferase assay shows the activities of a series of deleted constructs in both CHO and NIH-3T3 cells. Left panel shows each deleted mutant linked with the luciferase gene in the pGL3-basic vector. Right panel indicates the relative activities of these deleted constructs, as determined by luciferase assays. (**C**) Point mutation analysis of the core promoter using luciferase assays. The 259 bp LS7 construct was used as a basic construct for the point mutation analysis. Luciferase assays were used to determine the relative activities. The intact binding sites of the GC box, GATA-like element MBS1 and MBS2 are indicated by open boxes and by circles, respectively. The filled boxes and circles show corresponding mutations. The pGL3-basic vector was used as a negative control. The data are based on the luciferase activity of pGL3-LS7. The mean ± SD are from 3 independent experiments.*, $P < 0.05$; **, $P < 0.01$ compared with the LS7 wild-type construct. See also **Figure S3**.

cells, as revealed by RT-PCR and by western blot analyses (**Fig. 3F and G**). These results suggest that GATA1 and MYBL2 activate the *Vdac2* promoter.

Transcription factors GATA1 and MYBL2 bind to the *Vdac2* promoter both in vivo and in vitro

Chromatin immunoprecipitation analysis was performed to investigate whether the transcription factors SP1, GATA1, GATA2, and MYBL2 bind to the mouse *Vdac2* promoter in vivo. A 276 bp DNA region from anti-GATA1 or anti-MYBL2 antibody precipitates was amplified, which was not obtained from the anti-SP1 or anti-GATA2 antibody precipitates in the ovary (**Fig. 4A and B**). Sequencing analysis confirmed that the amplified fragments were *Vdac2* promoter-specific. Another DNA fragment in a distinct genomic region (exon7) was amplified as a control to exclude the possibility of nonspecific binding to the *Vdac2* promoter region. No band from the anti-SP1, anti-GATA1, anti-GATA2 or anti-MYBL2 antibody precipitates was observed. These results indicate that both GATA1 and MYBL2, but not SP1 and GATA2, specifically bind to the *Vdac2* promoter region in vivo.

Electrophoretic mobility shift assays were used to further determine whether the transcription factors GATA1 and MYBL2 bind to the GATA-like element and MBS of the promoter, respectively. A DNA-protein complex was detected

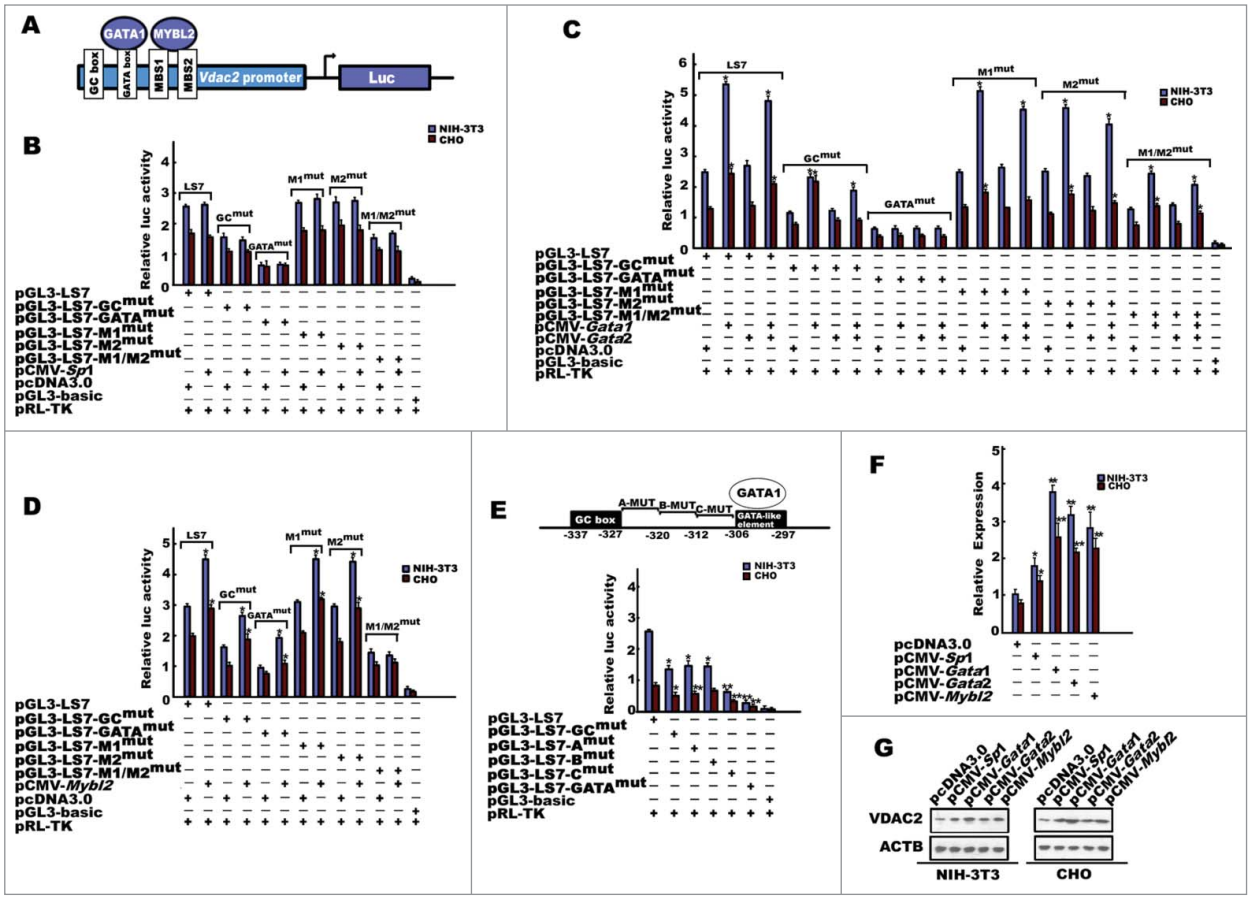

Figure 3. Overexpression of GATA1 and MYBL2 upregulates *Vdac2* promoter activity. (**A**) *Vdac2* promoter structure and luciferase activity measurement. (**B**) Overexpression of SP1 (predicted binding site: GC-box) does not contribute to *Vdac2*-luciferase activity. NIH-3T3 or CHO cells were transfected with 0.2 μg pGL3-LS7 or its several mutants (pGL3-LS7-GC^{mut}, pGL3-LS7-GATA^{mut}, pGL3-LS7-M1^{mut}, pGL3-LS7-M2^{mut}, and pGL3-LS7-M1/M2^{mut}) and the 0.2 μg SP1 expression plasmid (pCMV-*Sp1*), as indicated. (**C**) Overexpression of GATA1 activates the *Vdac2* promoter. In total, 0.2μg pGL3-LS7 or its several site mutants (pGL3-LS7-GC^{mut}, pGL3-LS7-GATA^{mut}, pGL3-LS7-M1^{mut}, pGL3-LS7-M2^{mut} and pGL3-LS7-M1/M2^{mut}) were cotransfected with 0.2 μg *Gata1* and *Gata2* expression plasmids (pCMV-*Gata1* and pCMV-*Gata2*), as indicated. GATA1 overexpression increases the activity of all the structures except pGL3-LS7-GATA^{mut}. GATA2 overexpression does not affect the activities of these structures. Overexpression of both GATA1 and GATA2 (0.1 μg) does not increase or decrease the activities compared with GATA1. (**D**) Promoter activities of 3 deleted constructs between the GC box and GATA-like element, as determined by luciferase assay. Each of the point mutations can decrease *Vdac2*-luciferase activity. Upper panel indicates the schematic depiction of mutants between the GC box and the GATA-like element. (**E**) Overexpression of MYBL2 upregulates *Vdac2* promoter activity. In total, 0.2μg pGL3-LS7 or its several site mutants (pGL3-LS7-GC^{mut}, pGL3-LS7-GATA^{mut}, pGL3-LS7-M1^{mut}, pGL3-LS7-M2^{mut} and pGL3-LS7-M1/M2^{mut}) were cotransfected with 0.2 μg *Mybl2* expression plasmid (pCMV-*Mybl2*). MYBL2 overexpression increases *Vdac2* promoter activity, except pGL3-LS7-M1/M2^{mut}. (**F**) Real-time RT-PCR shows that *Sp1, Gata1, Gata2*, or *Mybl2* overexpression can increase the transcription of the endogenous *Vdac2* gene in both NIH-3T3 and CHO cells. pcDNA3.0 was used as transfection control. *Actb* was used as an internal control. (**G**) Western blots show that SP1, GATA1, GATA2 or MYBL2 overexpression upregulates the endogenous VDAC2 protein level in both NIH-3T3 and CHO cells. ACTB served as an internal control.

when a GATA-like element probe spanning −314 bp to −295 bp was incubated with a mouse ovary nuclear extract. An excess amount of unlabeled oligo DNA, but not the mutated GATA-like element, could compete with this binding. Moreover, when the anti-SP1, anti-GATA1, or anti-GATA2 antibody was added to the binding reaction, the supershift band appeared only by adding the anti-GATA1 antibody (**Fig. 4C**). These results show that the transcription factor GATA1 can bind to the GATA-like element from −307 bp to −296 bp of the *Vdac2* promoter in vitro. A DNA-protein complex was generated when the nuclear extract was incubated with a probe that included 2 MBS sites spanning −289 bp to −260 bp. An excess amount of unlabeled oligo DNA or individual MBS-site mutant, but not the double-mutated MBS-site mutants, could compete with this binding. Moreover, the supershift band was detected by adding anti-MYBL2 antibody to the binding reaction (**Fig. 4D**). These results indicate that the 2 MBS sites from −289 bp to −260 bp of the *Vdac2* promoter are specific for binding the transcription factor MYBL2 in vitro.

MYBL2 regulates the spatiotemporal expression of *Vdac2* in the developing ovary

To determine the spatiotemporal consistency of both MYBL2 and VDAC2 expression during ovary development, we detected MYBL2 expression in comparison with VDAC2 expression in

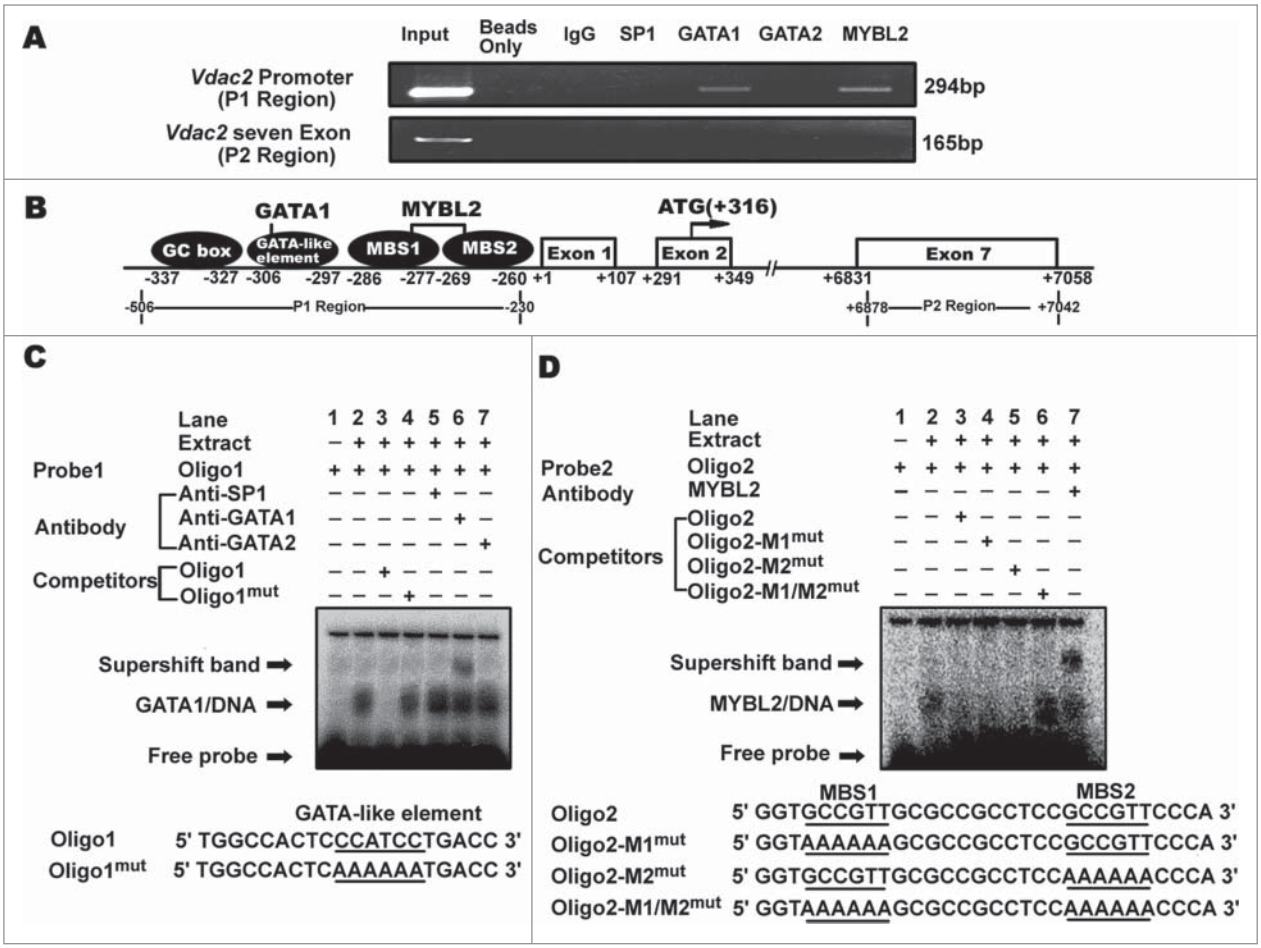

Figure 4. ChIP and EMSA assays of GATA1 and MYBL2 binding to the *Vdac2* promoter. (**A**) ChIP assay. Chromatin immunoprecipitation analysis shows that GATA1 and MYBL2 can bind to the *Vdac2* promoter in vivo; however, SP1 and GATA2 cannot bind. Sonicated chromatin from mouse ovary samples was immunoprecipitated with anti-SP1, anti-GATA1, anti-GATA2, anti-MYBL2, no antibody (beads only) or preimmune IgG (control). A 276 bp fragment corresponding to the −506 to −230 region of the *Vdac2* promoter was amplified using the immunoprecipitated DNA as a template. Exon 7 of *Vdac2* was used as a negative control. (**B**) Schematic diagram of primer relative positions in the ChIP assay. (**C**) EMSA assay showing GATA1 binding to the *Vdac2* promoter. Oligo1, corresponding to −314 to −295, was $\gamma-^{32}$P-ATP labeled and incubated with 15 μg of the mouse ovary nuclear extract in the absence or presence of a 50-fold excess of various competitor DNA oligos (mutant or unlabeled oligo1) or antibodies (GATA1, GATA2 or SP1), as indicated. The specific super-shift band (lane 6) is indicated by an arrow. The competitor mutated DNA cannot affect the DNA/protein complex formation (lane 4). The DNA sequences of oligo1 and the corresponding mutant are shown under the panel. (**D**) EMSA assay showing MYBL2 binding to *Vdac2* promoter. The DNA corresponding to −289 to −269 bp was $\gamma-^{32}$P-ATP labeled and incubated with the mouse ovary nuclear extract in the absence or presence of various competitor DNA oligos (50-fold excess, mutants or unlabeled oligo2) or antibody (MYBL2), as indicated. Arrow indicates the specific supershift band (lane 7). The DNA sequences of oligo2 and corresponding mutants are indicated under the panel. The DNA-protein complex formation can be affected by adding a 50-fold excess of unlabeled oligo2 (lane 3) and mutated DNA competitors for MBS1 and MBS2, respectively (lanes 4 and 5) but cannot be affected by adding both MBS1 and MBS2 double-mutated DNA competitors (lane 6).

the developing ovary. MYBL2 protein expression had the same trend as VDAC2, with a specific peak at 16 dpp (**Fig. 5A** and **B**). Notably, the immunofluorescence analysis showed that MYBL2 was expressed in the nuclei of stromal cells and primordial germ cells at 2 dpp. MYBL2 expression was obvious in the granulosa cells, oocytes, and basement membranes at 14 dpp. Then, MYBL2 was highly expressed in the oocytes and granulosa cells until adulthood, whereas its expression decreased in theca cells after 18 dpp (**Fig. 5A, B** and **S1**). In addition, GATA1 was consistently expressed from 2 dpp to adult. These data show that MYBL2 regulates a spatiotemporal expression of *Vdac2* in the developing ovary, suggesting a potential role for the MYBL2-VDAC2 pathway in follicle development.

The Ss*VDAC2* promoter exerts its function in transgenic ovaries

To investigate the function of the Ss*VDAC2* promoter in vivo, Ss*VDAC2*-transgenic pigs were generated using the porcine Ss*VDAC2* core promoter-driven Ss*VDAC2* CDS (coding DNA sequence) with a FLAG tag. Sequence comparison showed a highly conserved promoter with a GATA-like element and a MBS site between mouse and pig, and 5 GATA-like elements

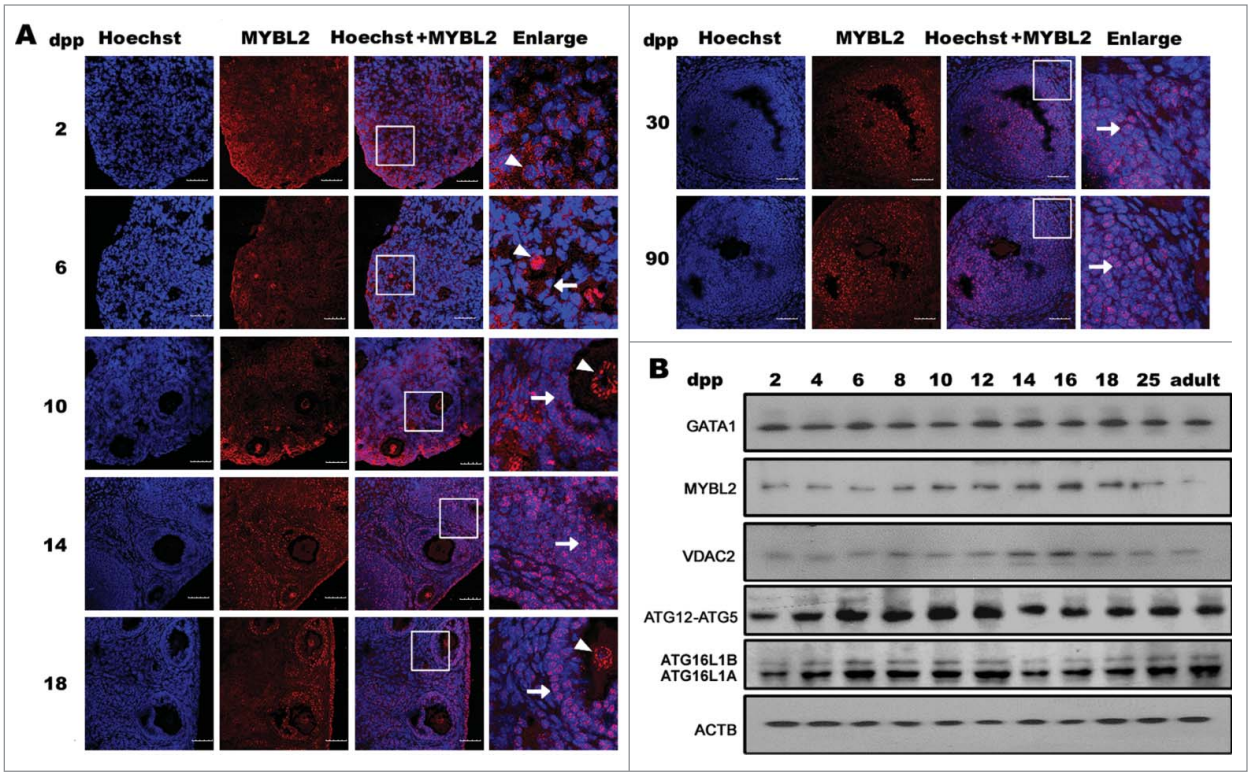

Figure 5. MYBL2 and GATA1 are expressed in the developing ovaries of postnatal mice. (**A**) MYBL2 immunolocalization in the developing ovaries of postnatal mice using the anti- MYBL2 antibody. MYBL2 is expressed in the nuclei of stromal cells and oocytes at 2 dpp; MYBL2 expression gradually increases from 6 dpp to 18 dpp in oocytes, theca and granulosa cells. After 18 dpp, MYBL2 maintains high expression in oocytes and granulosa cells but less in theca cells. The nuclei were stained with Hoechst reagent. The enlarged images originated from the white squares. The arrows indicate granulosa cells, whereas arrowheads indicate the oocytes. Scale bar: 50 μm. See also **Figure S1**. (**B**) Western blot analysis showing the GATA1, MYBL2, ATG5, and ATG16L1 protein levels in the developing ovaries of postnatal mice. The MYBL2 expression pattern is similar to VDAC2, with a peak at 16 dpp in the ovary. The ATG5 and ATG16L1 expressions in postnatal ovaries increased till 12 dpp and then decreased obviously after 14 dpp. The A and B isoforms of ATG16L1 were detected. ACTB was used as an internal control.

present in the porcine promoter (**Fig. 6A and C**). In addition, we detected 2 types of haplotypes (types J and Y) in the Ss*VDAC2* promoter. Haplotype Y had a higher frequency than type J in 2 breeds (Landrace and Hubei White), and the frequency of haplotype J was higher in Hubei White (litter size >12)[33] than in Landrace (litter size ~11)[34] (**Fig. 6A**). Promoter activities of the 2 types of haplotypes showed that the haplotype J promoter had slightly higher activity than the haplotype Y promoter (**Fig. 6B**). Thus, the haplotype J promoter was used to generate the transgenic pigs (**Fig. 6C**). Transfection and western blot analyses showed that the transgenic construct could be expressed in 293T cells (**Fig. 6D**). A transgenic male founder was generated, which was used to mate with a wild-type female, and 3 positive females were obtained in the F1 generation (**Fig. 6E and F**). In addition to 15 corpus albicans, 21 mature follicles (8, 8 to 10 mm; 13, 5 to 8 mm) were observed on the surface of both sides of ovaries from the positive female (F1-c') (**Fig. 6G to I**). The statistic analysis of different kinds of follicles on the serial sections of ovary showed more primary follicles, but less atretic follicles in the Ss*VDAC2* transgene than in wild-type ovaries (**Fig. 6J**). To further examine Ss*VDAC2* transgene expression, immunofluorescence and confocal microscopy were used to analyze on the transgenic ovary sections. SsVDAC2 and FLAG proteins were expressed in the cytoplasm of the granulosa cells and oocytes, whereas SsMYBL2 was expressed in the nuclei of the granulosa cells, similar to those expression patterns observed in mice (**Fig. 6K** and **S4**). These data suggest that endogenous GATA1 activates the primary expression of VDAC2 and MYBL2 upregulates VDAC2 expression in the developing ovary; thus, the Ss*VDAC2* promoter can exert its function in the transgenic ovary.

SsVDAC2 overexpression inhibits autophagy in the Ss*VDAC2* transgenic ovary

To investigate a potential role of VDAC2 in autophagy in the ovary, we examined SsLC3B-II (the cleaved, lipidated, and autophagosome-bound form of the key autophagy protein, LC3B) in the Ss*VDAC2* transgenic ovary. Western blot analysis showed that both endogenous and SsVDAC2 transgenic proteins were expressed in the transgenic ovary. Notably, SsLC3B-II was downregulated in the Ss*VDAC2* transgenic pig ovary in comparison with the wild-type ovary. In addition, SsATG16L1 and SsATG12-n nSsATG5 were also downregulated in the transgenic ovary (**Fig. 7A**). Because no downregulation of either Ss*ATG5* or

Ss*ATG16L1* mRNA was detected in the Ss*VDAC2* transgenic ovary (**Fig. 7B**), we determined whether both SsATG5 and SsATG16L1 proteins were degraded by ubiquitination. When VDAC2 was overexpressed in 293T cells, both ATG5 and ATG16L1 proteins were obviously ubiquitinated (**Fig. 7C**). In the Ss*VDAC2* transgenic ovary, ubiquitination of the proteins was also detected (**Fig. 7D and E**). Immunofluorescence analysis indicated that SsLC3B was primarily expressed in the cytoplasm of both granulosa cells and oocytes in both transgenic and wild-type ovaries (**Fig. 7F**). In addition, SsLC3B expression was slightly decreased in the granulosa cells in the Ss*VDAC2* transgenic ovary compared with the wild-type ovary (**Fig. 7F**). Obvious SsLC3-puncta were detected in the internal theca cell layer in the follicle from the wild-type ovary compared with the transgenic ovary (**Fig. 7G**). Because VDAC2 interacts with proapoptotic protein BAK1 (BCL2-antagonist/killer 1), which inhibited apoptosis,[22] we also determined whether apoptosis occurred in the Ss*VDAC2* transgenic ovaries. Indeed, obvious FITC-labeled apoptosis signals in the theca cell layer of mature follicles were detected in wild-type compared to the transgenic ovaries (**Fig. S5**), indicating that the Ss*VDAC2* transgene inhibited apoptosis, in addition to autophagy suppression. These results suggest that Ss*VDAC2* overexpression not only decreases SsLC3B-II, SsATG16L1, and SsATG12-SsATG5 protein levels in the ovary and inhibits autophagosome formation, but also suppresses apoptosis in the theca cell layer of mature follicles.

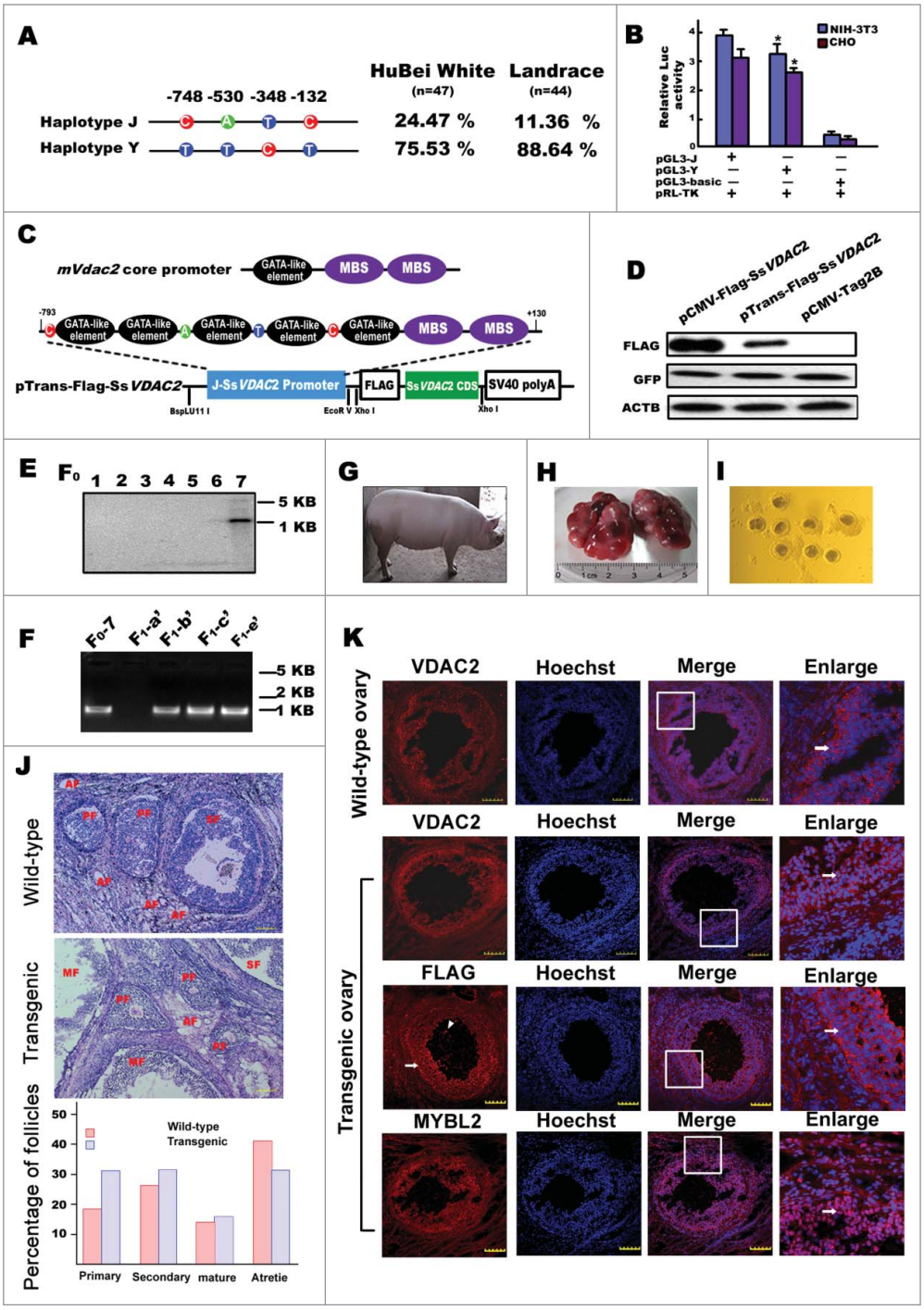

Figure 6. For figure legend, see page 1089.

***Vdac2* knockout (*vdac2*$^{-/-}$) promotes autophagy**

To further examine a role for *Vdac2* in regulating autophagy, *vdac2*$^{-/-}$ MEF cells were used to detect autophagosome formation under starvation conditions because the *Vdac2* knockout mouse is lethal.[22] Obvious LC3 puncta were detected at 1 h under starvation culture conditions in *vdac2*$^{-/-}$ cells, whereas LC3 puncta appeared at 3 h under starvation conditions in wild-type cells. When *Vdac2* expression was rescued in *vdac2*$^{-/-}$cells by infecting them with lentivirus expressing *Vdac2*, obvious LC3-puncta appeared again at 3 h under starvation conditions (**Fig. 8A to C**). Western blot analysis confirmed that LC3B-II, which is the autophagosome-bound form of the key autophagy

protein LC3B, was upregulated in *vdac2*$^{-/-}$cells under starvation conditions in comparison with the normal culture conditions (**Fig. 8D**). In addition, ATG16L1 and ATG12–ATG5 were also upregulated in *vdac2*$^{-/-}$ cells under starvation conditions. These results suggest that VDAC2 downregulates autophagy.

VDAC2 inhibits autophagy by interacting with BECN1 and BCL2L1 to stabilize the BECN1 and BCL2L1 complex

To investigate the roles of VDAC2 in the autophagy regulation pathway, the VDAC2-interacting proteins involved in autophagy initiation were identified using coimmunoprecipitation and colocalization analyses. We determined that BECN1, which is a key protein for autophagy initiation, could clearly interact with VDAC2 in 293T cells (**Fig. 9A**). Deletion and truncation mutation analyses showed that VDAC2 bound to the N terminus of BECN1, but not to the BH3, CCD, or ECD domains (**Fig. 9C, D and F**). Both BECN1 and its N-terminal region had obvious colocalization with VDAC2 (**Fig. 9B, E and G**). A possible interaction of VDAC2 with BCL2 and BCL2L1 was further examined because BECN1 can interact with BCL2L1 and BCL2 and inhibit autophagy initiation.[13,35] The coimmunoprecipitation analysis indicated that VDAC2 interacted with BCL2L1 but not BCL2 (**Fig. 10A**) and that VDAC2 also colocalized with BECN1 and BCL2L1 in HeLa cells (**Fig. 10B**). We further confirmed the interactions of these 3 proteins in vivo. Coimmunoprecipitation analysis showed that VDAC2 can interact with BECN1 and BCL2L1 in mouse ovary (**Fig. 10C–E**).

To further investigate the interaction modes of VDAC2, BECN1 and BCL2L1, a coimmunoprecipitation analysis was performed, which indicated that the 3 proteins formed a complex to stabilize each other (**Fig. 10F** and **11A**). However, N-terminal deletion of BECN1 showed that VDAC2 did not promote BECN1 interaction with BCL2L1 when the interaction between VDAC2 and BECN1 did not exist (**Fig. 10G**). Both deletion and point mutations in the BECN1 BH3 domain showed that BECN1 inhibited BCL2L1 interaction with VDAC2 and that BCL2L1 did not promote the VDAC2 interaction with the mutated BH3 domain of BECN1 (**Fig. 11B to D**). Taken together, these results suggest that VDAC2 inhibits autophagy by enhancing its interaction with BECN1 and BCL2L1 (**Fig. 11E**).

Discussion

Folliculogenesis is an essential process for producing functional eggs for fertilization in mammals. Because the total number of ovarian follicles is determined early in life,[36,37] accurate regulation of follicular development from primordial to mature follicles is important for females. However, the molecular mechanisms underlying folliculogenesis are not completely understood. In this study, we provide several key findings to outline a putative contribution of autophagy suppression to folliculogenesis in mammals.

We identified key regulators for VDAC2 expression in the developing ovary. Notably, both GATA1 and MYBL2 bound to and activated the *Vdac2* promoter. MYBL2 regulated the spatiotemporal expression of VDAC2, with a peak expression level at 14 dpp in the developing ovary, which is a key stage for the developmental transition from primary to secondary follicles.[38] The function of the VDAC2 in the developing ovary was further confirmed in Ss*VDAC2* transgenic pigs. A bovine cDNA microarray analysis has indicated that *VDAC2* is expressed in dominant follicles.[39] Our recent study demonstrates that Ss*VDAC2* is also upregulated during long-term litter size selection in pigs.[32] These data support our observation of a role of VDAC2 in the mammalian ovary.

Importantly, we revealed that VDAC2 exerts its functions in the developing ovary as an autophagy suppressor. SsLC3B-II was downregulated in the Ss*VDAC2* transgenic pig ovary compared to the wild-type ovary. Specifically, SsLC3-positive autophagosome formation was inhibited in the Ss*VDAC2* transgenic ovary. Moreover, SsATG16L1 and SsATG12-SsATG5, which are key proteins for autophagy membrane formation, were also downregulated in the Ss*VDAC2* transgenic ovary. Notably, LC3B II was upregulated in *vdac2*$^{-/-}$ cells under starvation-induced autophagy. Our data suggest that VDAC2 inhibits autophagy at the initiation of autophagosome formation. Because the *Vdac2*

Figure 6. (See previous page). Transgenic pig analysis. (**A**) Identification of promoter haplotypes of the porcine (*Sus scrofa*/Ss) *VDAC2* gene. Schematic depiction shows the relative positions of the SNPs in 2 types of haplotypes (J and Y). The right panel shows haplotype frequencies in 2 breeds (Landrace and Hubei White). (**B**) Promoter activities of 2 types of haplotypes, as determined by luciferase assays. The haplotype J promoter has higher activity than the haplotype Y promoter does. (**C**) Schematic depiction of the pTrans-Flag-Ss*VDAC2* transgenic construct. This transgenic structure contains a region of the haplotype J promoter from −793 bp to +130 bp and the Ss*VDAC2* CDS with a *Flag* tag cloned into the pCMV-Tag2B vector. The Ss*VDAC2* promoter has 5 GATA-like elements and 2 MBS sites, similar to the core promoter of mouse *Vdac2*. (**D**) Western blot analysis shows the expression of the transgenic construct pTrans-Flag-Ss*VDAC2* in 293T cells. The cells were transiently transfected with pCMV-Flag-Ss*VDAC2*, pTrans-Flag-Ss*VDAC2* or pCMV-Tag2B with pEGFP-N1. The proteins were detected using the anti-FLAG antibody, and GFP and ACTB were used as controls. (**E**) Southern blot analysis shows the Ss*VDAC2*-positive transgenic male (F_0–7). (**F**) Identification of the transgenic offspring (F_1) by PCR. Three transgenic females were identified (F_1-b′, -c′ and -e′). (**G**) A photo of the female heterozygote F_1-c′. (**H**) The ovary image of F_1-c′ highlights many mature follicles. (**I**) Mature oocytes isolated from the F1-c′ ovary. (**J**) Histological analysis of Ss*VDAC2* transgenic and wild-type ovaries. The H.E. staining shows different stages of follicles. The statistic analysis of different stage of follicles from 60 sections for each ovary shows more primary follicles, but less atretic follicles in Ss*VDAC2* transgenic than in wild-type ovaries. PF, primary follicles; SF, secondary follicles; MF, mature follicles; AF, atretic follicles. Scale bar: 100 μm. (**K**) Immunofluorescence analysis of the Ss*VDAC2* transgenic ovary. SsVDAC2 expression in the wild-type ovary was examined by indirect immunofluorescence as a control. Transgenic FLAG-SsVDAC2, endogenous SsVDAC2 and SsMYBL2 proteins were examined by indirect immunofluorescence and by confocal microscopy using anti-VDAC2, anti-FLAG and anti-MYBL2 antibodies. SsVDAC2 and FLAG proteins were expressed in the cytoplasm of the granulosa cells and oocytes, whereas SsMYBL2 was expressed in the nuclei of the granulosa cells. The arrows indicate granulosa cells, and arrowheads show the oocytes. Scale bar: 100 μm. See also **Figure S4**.

knockout mouse is lethal,[22] *Atg5*-deficient mice die after within one d after birth[40] and oocyte-specific *Atg5*-knockout mice also lead embryonic lethality at the 4-cell to 8-cell stages,[41] further development of *Vdac2* conditional knockout in specific cell types of ovary will aid us in understanding of molecular mechanisms of these proteins in oogenesis.

We identified a VDAC2 pathway that regulates autophagy. VDAC2 could interact with both BECN1 and BCL2L1 to

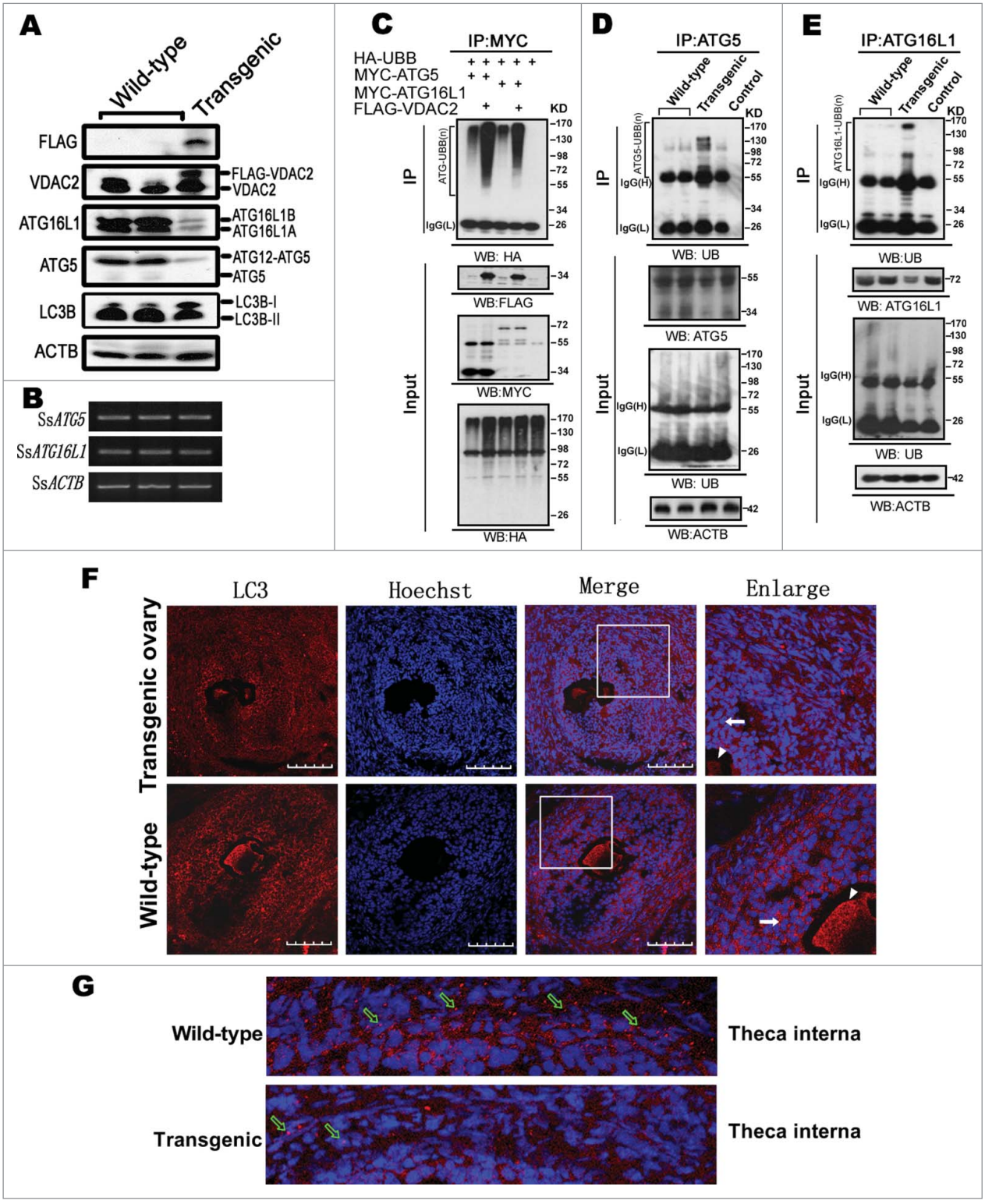

Figure 7. For figure legend, see page 1091.

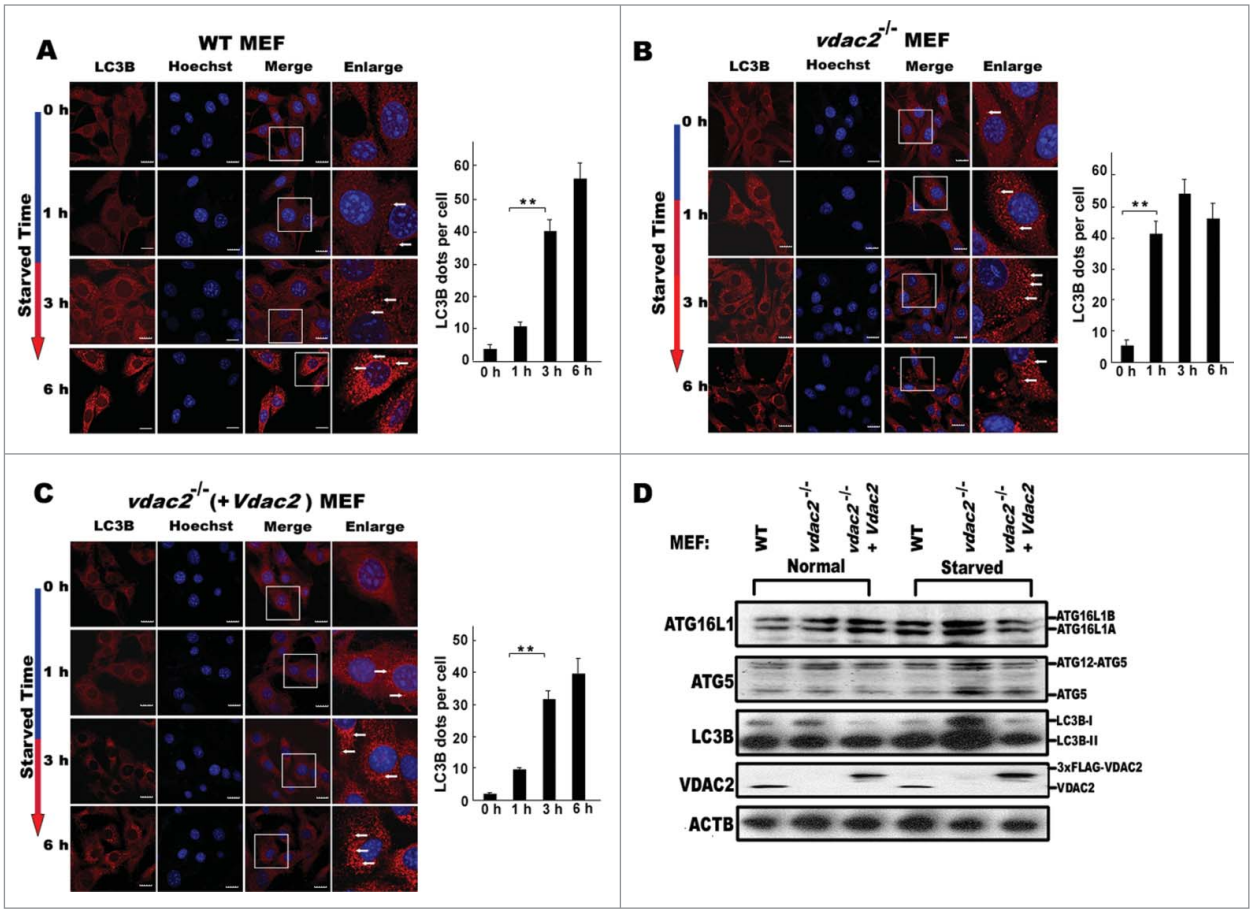

Figure 8. *Vdac2* knockout (*vdac2*$^{-/-}$) promotes autophagy. (**A**) Obvious LC3-puncta are detected in WT MEF cells after starvation culture conditions (DMEM with no serum) for 3 h. The cells were cultured in DMEM with no serum for the indicated time and analyzed by immunofluorescence with the anti-LC3B antibody and by confocal microscopy. The enlarged images originated from the squares in the merge panel, highlighting red LC3 puncta in the cytoplasm. The nuclei were stained with Hoechst reagent. Arrows indicate LC3 signals. Scale bar: 20 μm. The numbers of LC3B dots in 30 cells were counted for each group. (**B**) Obvious LC3-puncta appear at 1 h under starvation culture conditions in the *vdac2*$^{-/-}$ cells. (**C**) To rescue *Vdac2* expression in the *vdac2*$^{-/-}$ cells, the cells were infected with lentivirus expressing 3xFLAG-VDAC2 and analyzed by immunofluorescence with the anti-LC3B antibody. Obvious LC3-puncta appear again at 3 h under starvation-culture conditions. Scale bar: 20 μm. (**D**) Western blot analysis showing that *vdac2*$^{-/-}$ promotes autophagy under starvation conditions. The WT MEF, *vdac2*$^{-/-}$ MEF, and the 3xFLAG-VDAC2 rescued *vdac2*$^{-/-}$ MEF were cultured in DMEM with no serum for 3 h and analyzed by western blotting with the anti-LC3B, anti-VDAC2, anti-ATG16L1, anti-ATG5 and anti-ACTB antibodies. LC3-II, the cleaved and lipidated form of the autophagy protein LC3B is a widely known marker of autophagy.

inhibit autophagy. VDAC2 is a mitochondrial protein, which is expressed ubiquitously and enriched in granulosa cells. BCL2L1 and BECN1 are also localized in granulosa cells in mammals and chicken.[42-44] Taken together, our results reveal that VDAC2 inhibits autophagy by enhancing the interaction between BECN1 and BCL2L1 in ovary when autophagy is inactivated,

Figure 7. (See previous page). Downregulation of autophagy in the Ss*VDAC2* transgenic ovary. (**A**) Western blot analysis showing that SsLC3B-II, SsATG12-SsATG5, and SsATG16L1 were downregulated in the Ss*VDAC2* transgenic pig ovary in comparison with the wild-type ovary. Both endogenous and transgenic FLAG-VDAC2 were expressed in the ovary. ACTB and FLAG were used as the controls. (**B**) Semiquantitative PCR shows that Ss*ATG5* and Ss*ATG16L1* have unchanged RNA levels in the Ss*VDAC2* transgenic ovary in comparison with the wild-type ovary. (**C**) Overexpression of VDAC2 promotes ATG5 and ATG16L1 ubiquitination in 293T cells. pFlag-*Vdac2*, pHA-*Ubb* and pMyc-*Atg5* or pMyc-*Atg16l1* were transfected into the cells as indicated. Coimmunoprecipitation assays were performed with anti-MYC antibody. Western blots were analyzed with an anti-FLAG, anti-HA or anti-MYC antibody. (**D**, **E**) The ubiquitination levels of SsATG5 (**D**) and SsATG16L1 (**E**) were higher in transgenic than in wild-type ovaries. Coimmunoprecipitation assays were performed with anti-ATG5 or anti-ATG16L1 antibody using ovary lysates. Western blots were analyzed with anti-UB, anti-ATG5, anti-ATG16L1, or anti-ACTB antibody. (**F**) Immunofluorescence analysis of the SsLC3B protein in the transgenic and wild-type pig ovaries using the anti-LC3B antibody. SsLC3B is primarily expressed in the cytoplasm of both granulosa cells and oocytes in both transgenic and wild-type ovaries. SsLC3B expression is slightly decreased in granulosa cells of the Ss*VDAC2* transgenic ovary in comparison with the wild-type ovary. The nuclei were stained with Hoechst reagent. The enlarged images originated from the white squares. The arrows indicate granulosa cells, whereas arrowheads indicate the oocytes. Scale bar: 100 μm. (**G**) Images highlight the theca interna from panel (**F**). Obvious SsLC3-puncta are detected in the theca interna layer in the follicle from the wild-type ovary compared with the transgenic ovary. The blank arrows indicate SsLC3-puncta.

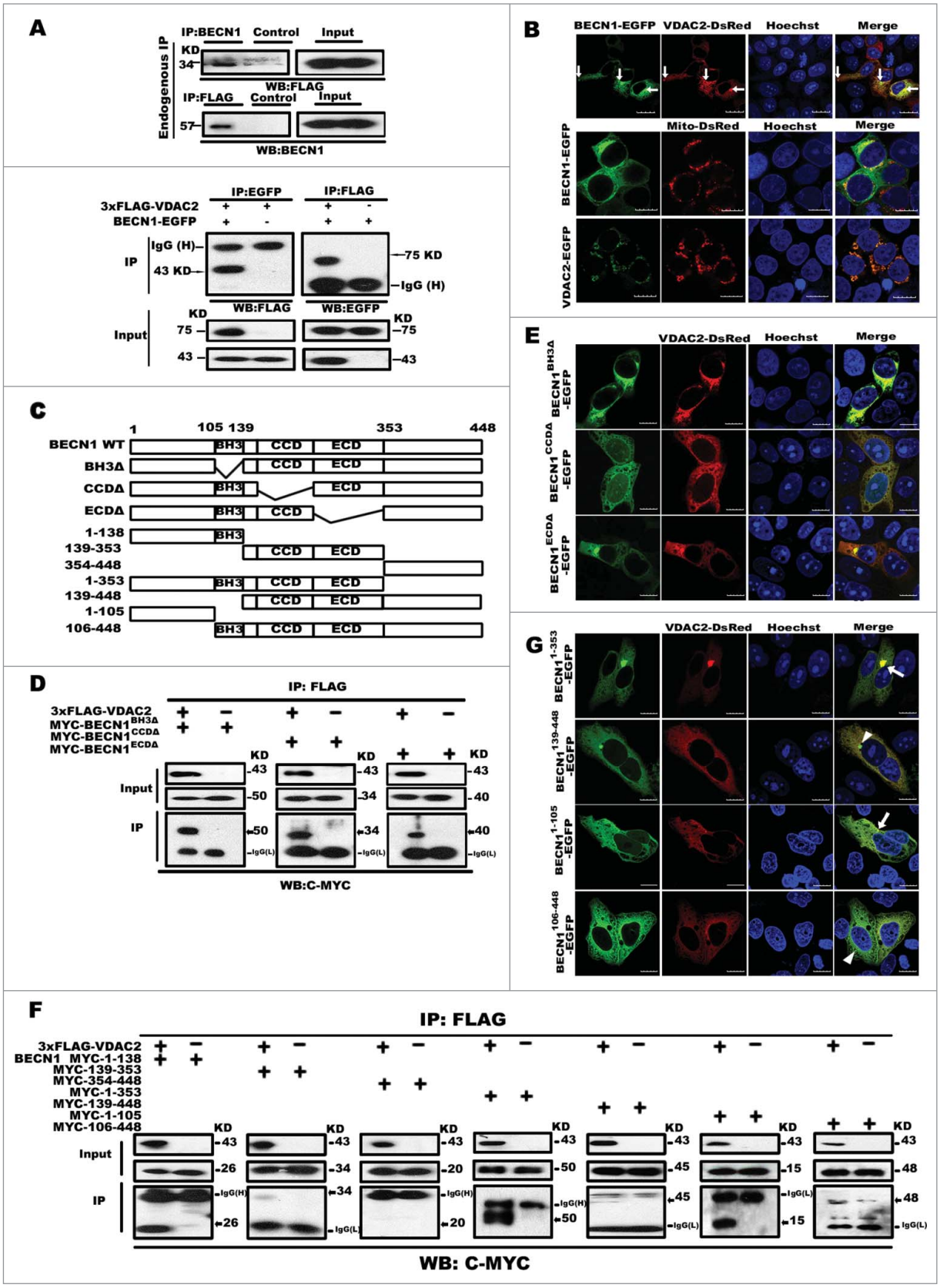

Figure 9. For figure legend, see page 1093.

whereas VDAC2 interaction with BECN1 promotes BCL2L1 separation from the triple complex when autophagy induces BECN1 and BCL2L1 dissociation.[45,46]

Autophagy could aid oogenesis in accurately regulating follicular atresia and dominant follicle development. Autophagy is observed in rat ovary, which is also associated with apoptosis.[20] We suggest that VDAC2 may exert its functions in follicle development through enhancing its interaction with BECN1 and BCL2L1, not only to inhibit autophagy, but also to suppress apoptosis in the theca cell layer of the mature follicles. Thus, VDAC2 is a dual-functional factor in regulation of autophagy and apoptosis, which may collaborate in regulating follicular development.

We have demonstrated the interaction between VDAC2 and BECN1, which has a BH3 domain.[13] Although VDAC2 directly interacts with the BH3 domain-only BCL2 family member BAK1,[22] the VDAC2 interaction with BECN1 occurred at the N terminus but not with the BH3 domain. BECN1, which is an important autophagy protein, has a low expression level in human breast epithelial carcinoma cells and promotes autophagy in human MCF7 breast carcinoma cells when transfected.[47] BECN1-defective mice die early during embryogenesis, and a high frequency of spontaneous tumors occurs in BECN1-heterozygous mice.[48,49] The ovaries of BECN1-heterozygous mice show a substantial reduction of germ cells.[42] These data suggest a role of the VDAC2 and BECN1 interaction during autophagy regulation for folliculogenesis.

Moreover, our results showed that VDAC2 interacted with BCL2L1 but not BCL2. Previous studies have shown that the interaction between BCL2 and BCL2L1 with BECN1 is important for autophagy initialization.[45,46] BCL2 or BCL2L1 can directly bind to the BH3 domain of BECN1 to inhibit BECN1-dependent autophagy[13,14,50] and stabilization or dissociation of the BCL2-BECN1 or BCL2L1-BECN1 complex can inhibit or initiate autophagy.[14,51,52] Taken together, these observations suggest that VDAC2 interacts with both BECN1 and BCL2L1 to inhibit autophagy. Our results provide evidence for the molecular mechanisms of regulating VDAC2 expression in mammalian ovaries and reveal that VDAC2 exerts its function in autophagy suppression through interacting with BECN1 and BCL2L1 during formation of autophagosome membrane. These findings have potential implications in improving female fecundity through autophagy suppression pathways.

Materials and Methods

In silico sequence analysis

The TFSEARCH program (http://www.cbrc.jp/research/db/TFSEARCH.html) was used to predict the transcription factor binding sites in the promoters of both mouse *Vdac2* and pig *VDAC2* (Ss*VDAC2*). MethPrimer software (http://www.urogene.org/methprimer/index1.html) was used to predict the CpG islands in the *Vdac2* promoter with observed/expected ratios > 0.8 and with C+G > 50%.

Plasmid constructs

Eleven deletion fragments of the mouse *Vdac2* promoter were amplified from mouse genomic DNA, which were double-digested with *Mlu*I and *Xho*I and cloned into the pGL3-basic vector (Promega, E1751). The primers and PCR conditions are described in **Table S1**. Site-directed mutagenesis for the GC box, GATA-like element, and MBS was performed using the primers described in **Table S1**. A MBS1 mutant was used as the template for constructing both MBS1 and MBS2 mutants. For 2 haplotypes of *Vdac2* promoter vectors, pGL3-J and pGL3-Y were constructed using PCR, with pig genomic DNA as the template and with primers described in **Table S1**. The PCR products were double-digested with *Mlu*I and *Xho*I and cloned into the pGL3-basic vector. For constructing the transgenic vector pTrans-Flag-Ss*VDAC2*, the haplotype J promoter was cloned from pig genomic DNA using primers described in **Table S1**. The fragments were double-digested with *Bsplu*11I and *EcoR*V and cloned into the pCMV-Tag2B vector (1st vector). The Ss*VDAC2* CDS was amplified using pig cDNA as the template

Figure 9 (See previous page). VDAC2 interacts with BECN1. (**A**) 293T cells were transiently transfected with pFlag-*Vdac2* or both p*Becn1*-EGFP and p3xFlag-*Vdac2*, and after transfection for 48 h, the whole cell lysate was extracted for coimmunoprecipitation with anti-FLAG (mouse IgG for control), anti-BECN1 or anti-GFP (rabbit IgG for control). Anti-BECN1, anti-GFP or anti-FLAG antibody (input) was used for western blotting. (**B**) Colocalization analysis of VDAC2 and BECN1. HeLa cells were transiently cotransfected with p*Becn1*-EGFP and p*Vdac2*-DsRed, followed by confocal microscopy. Colocalizing structures are indicated in yellow (merge), and the white arrows show the overlapping signals in the cells. HeLa cells were transiently cotransfected with both p*Becn1*-EGFP and pMito-DsRed or both p*Vdac2*-EGFP and pMito-DsRed to show localization of BECN1 or VDAC2 as controls. (**C**) Schematic diagram of the mouse BECN1 wild type and various deletion and truncated mutants. The conserved domains (BH3, CCD and ECD) are indicated in boxes. (**D**) Coimmunoprecipitation between VDAC2 and deletion mutants of BECN1 domains. p3xFlag-*Vdac2* was transiently cotransfected with pMyc-*Bech1*$^{BH3\Delta}$, pMyc-*Becn1*$^{CCD\Delta}$, or pMyc-*Becn1*$^{ECD\Delta}$ in 293T cells. Cell lysates were examined by western blotting using the anti-MYC or anti-FLAG antibody (input). For coimmunoprecipitation, the lysates were immunoprecipitated with anti-FLAG, followed by immunoblotting with the anti-MYC antibody. All the domain-deletion mutants of BECN1 interact with VDAC2. (**E**) Colocalization analysis between VDAC2 and deletion mutants of BECN1 domains. HeLa cells were transiently cotransfected with p*Vdac2*-DsRed and p*Becn1*$^{BH3\Delta}$-EGFP, p*Vdac2*-DsRed and p*Becn1*$^{CCD\Delta}$-EGFP, or p*Vdac2*-DsRed and p*Becn1*$^{ECD\Delta}$-EGFP. Colocalizing structures are indicated in yellow (merge). (**F**) Coimmunoprecipitation analysis shows that VDAC2 interacts with the N terminus of BECN1. 3xFLAG-VDAC2 was cotransfected with pMyc-*Becn1*$^{1\ to\ 138}$, pMyc-*Becn1*$^{139\ to\ 353}$, pMyc-*Becn1*$^{354\ to\ 448}$, pMyc-*Becn1*$^{1\ to\ 353}$, pMyc-*Becn1*$^{139\ to\ 448}$, pMyc-*Becn1*$^{1\ to\ 105}$, or pMyc-*Becn1*$^{106\ to\ 448}$ into 293T cells. The cell lysates were examined by western blotting using the anti-MYC or anti-FLAG antibody (input). For coimmunoprecipitation, the lysates were immunoprecipitated with the anti-FLAG antibody, followed by immunoblotting with the anti-MYC antibody. FLAG-VDAC2 can interact with MYC-BECN1$^{1\ to\ 138}$, MYC-BECN1$^{1\ to\ 353}$, and MYC-BECN1$^{1\ to\ 105}$. (**G**) Colocalization analysis of VDAC2 with BECN1 truncated mutants. VDAC2-DsRed was transiently cotransfected with BECN1$^{1\ to\ 353}$-EGFP, BECN1$^{139\ to\ 448}$-EGFP, BECN1$^{1\ to\ 105}$-EGFP or BECN1$^{106\ to\ 448}$-EGFP in HeLa cells. Colocalizing structures are indicated in yellow (merge). Arrows indicate that the signals overlapped between BECN1 and VDAC2. The nuclei were stained with Hoechst reagent. Scale bar: 10 μm.

and primers described in **Table S1**, then double-digested with *Hind*III and *Xho*I, and cloned into the pCMV-Tag2B vector (2nd vector). The Ss*VDAC2* CDS (NM_214369.1) and the *Flag* tag were amplified using the PCR product from the second vector and primers. PCR fragments were digested with *Xho*I and cloned into the first vector. Mouse *Vdac2* CDS (NM_011695.2) was cloned into pDsRed-N1, pcDNA3.0-myc and pcmvTag2B using *Eco*RI and *Xho*I to generate VDAC2-RFP, MYC-VDAC2 and FLAG-VDAC2 fusion proteins, respectively and was cloned into psi-3xFlag-C1 using *Xho*I to generate psi-3xFlag-*Vdac2*. Full-length *Becn1* (NC_000080.6) was cloned into pEGFP-N1 (Clontech, GM-1013P031) and pcDNA3.0-myc using *Eco*RI and *Xho*I to generate p*Becn1*-EGFP and pMyc-*Becn1*, respectively. The *Becn1* fragments consisting of MYC-BECN1 residues 1 to 138, 139 to 353, 354 to 448, 1 to 353,139 to 448, 1 to 105, and 106 to 448 were amplified using PCR primers described in **Table S1**. The fragments were digested with *Eco*RI and *Xho*I and ligated into pcDNA3.0-myc and pEGFP-N1, respectively. A 2-step PCR-based mutagenesis method was used to construct *Becn1* deletion mutants lacking the BH3, CCD or ECD domain. Two partially overlapping fragments were amplified by primers *Becn1*$^{BH3\Delta}$-F and Myc-*Becn1*-R, Myc-*Becn1*-F and *Becn1*$^{BH3\Delta}$-R using pMyc-*Becn1* as the template in the first-step PCR. Two DNA fragments from step one were annealed and used as the template for the second-step PCR. The primers Myc-*Becn1*-F and Myc-*Becn1*-R were used to obtain the *Becn1*$^{BH3\Delta}$ mutant. The resulting PCR product was cloned into pcDNA3.0-myc and pEGFP-N1 to obtain pMyc-*Becn1*$^{BH3\Delta}$ and p*Becn1*$^{BH3\Delta}$-EGFP, respectively. Using the corresponding primers described in **Table S1**, The fusion-protein constructs MYC-BECN1$^{CCD\Delta}$, BECN1$^{CCD\Delta}$-EGFP, MYC-BECN1$^{ECD\Delta}$, and BECN1$^{ECD\Delta}$-EGFP were generated in the same way. The L114A and F121A point mutations of *Becn1* were generated by a 2-step PCR-based mutagenesis method using pMyc-*Becn1* as the template, and the resulting PCR product was cloned into pcDNA3.0-myc to obtain the mutated proteins MYC-BECN1^{L114A} and MYC-BECN1^{F121A}. Full-length *Bcl2l1* (NC_000068.7) and *Bcl2* (NC_000067.6) were cloned into pcDNA3.0-myc and pcmvTag2B using *Eco*RI and *Xho*I to generate the fusion proteins MYC-BCL2L1 and FLAG-BCL2L1, respectively. All constructs were sequenced. HA-UBB (ubiquitin B),

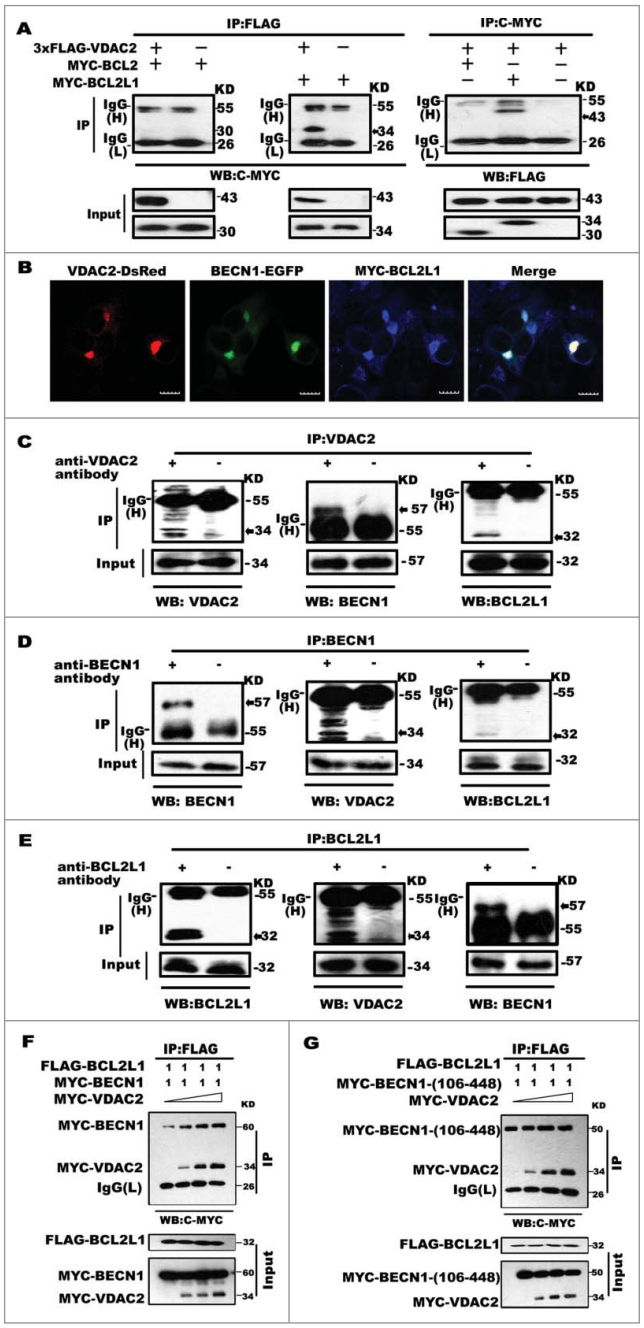

Figure 10. VDAC2 promotes BECN1 interaction with BCL2L1. (**A**) VDAC2 interaction with BCL2L1 but not BCL2. 3xFLAG-VDAC2 was transiently cotransfected with pMyc-*Bcl2* or pMyc-*Bcl2l1* into 293T cells. The lysates were immunoprecipitated with the anti-MYC or anti-FLAG antibody, followed by immunoblotting with the anti-FLAG or anti-MYC antibody, respectively. The whole cell lysates were examined by western blotting using the anti-MYC or anti-FLAG antibody (input). (**B**) Colocalization of VDAC2, BCL2L1 and BECN1. HeLa cells were cotransfected with p*Vdac2*-DsRed, p*Becn1*-EGFP and pMyc-*Bcl2l1*, followed by confocal microscopy. The MYC-BCL2L1 protein was detected by immunoblotting with the anti-MYC antibody (blue). Merged yellow signals indicate colocalizing structures (white arrows). Scale bar: 10 μm. (**C** to **E**) Coimmunoprecipitation analysis of interaction among VDAC2, BECN1 and BCL2L1 in mouse ovary. (**C**) The mouse ovary lysates were immunoprecipitated with anti-VDAC2, followed by immunoblotting with the anti-VDAC2, anti-BECN1 or anti-BCL2L1 antibody. (**D**) The mouse ovary lysates were immunoprecipitated with anti-BECN1, followed by immunoblotting with the anti-VDAC2, anti-BECN1 or anti-BCL2L1 antibody. (**E**) The mouse ovary lysates were immunoprecipitated with anti-BCL2L1, followed by immunoblotting with the anti-VDAC2, anti-BECN1, or anti-BCL2L1 antibody. (**F**) VDAC2 promotes the BECN1 interaction with BCL2L1. pMyc-*Vdac2* (0, 0.3, 0.6,and 1.2μg) was cotransfected with 1μg pFlag-*Bcl2l1* and 1 μg pMyc-*Becn1* into 293T cells. The cell lysates were immunoprecipitated with anti-Flag followed by immunoblotting with anti-MYC antibody. The whole cell lysates were examined by western blotting using the anti-MYC or anti-FLAG antibody (input). (**G**) pMyc-*Vdac2* (0, 0.3, 0.6, and 1.2 μg) cotransfected with pFlag-*Bcl2l1* (1 μg) and the BECN1 N-terminal deletion mutant (pMyc-*Becn1*$^{106\ to\ 448}$) (1 μg) into 293T cells. Coimmunoprecipitation was performed as in panel (**F**). VDAC2 promotion to the interaction between FLAG-BCL2L1 and the BECN1 N-terminal deletion mutant was not detected.

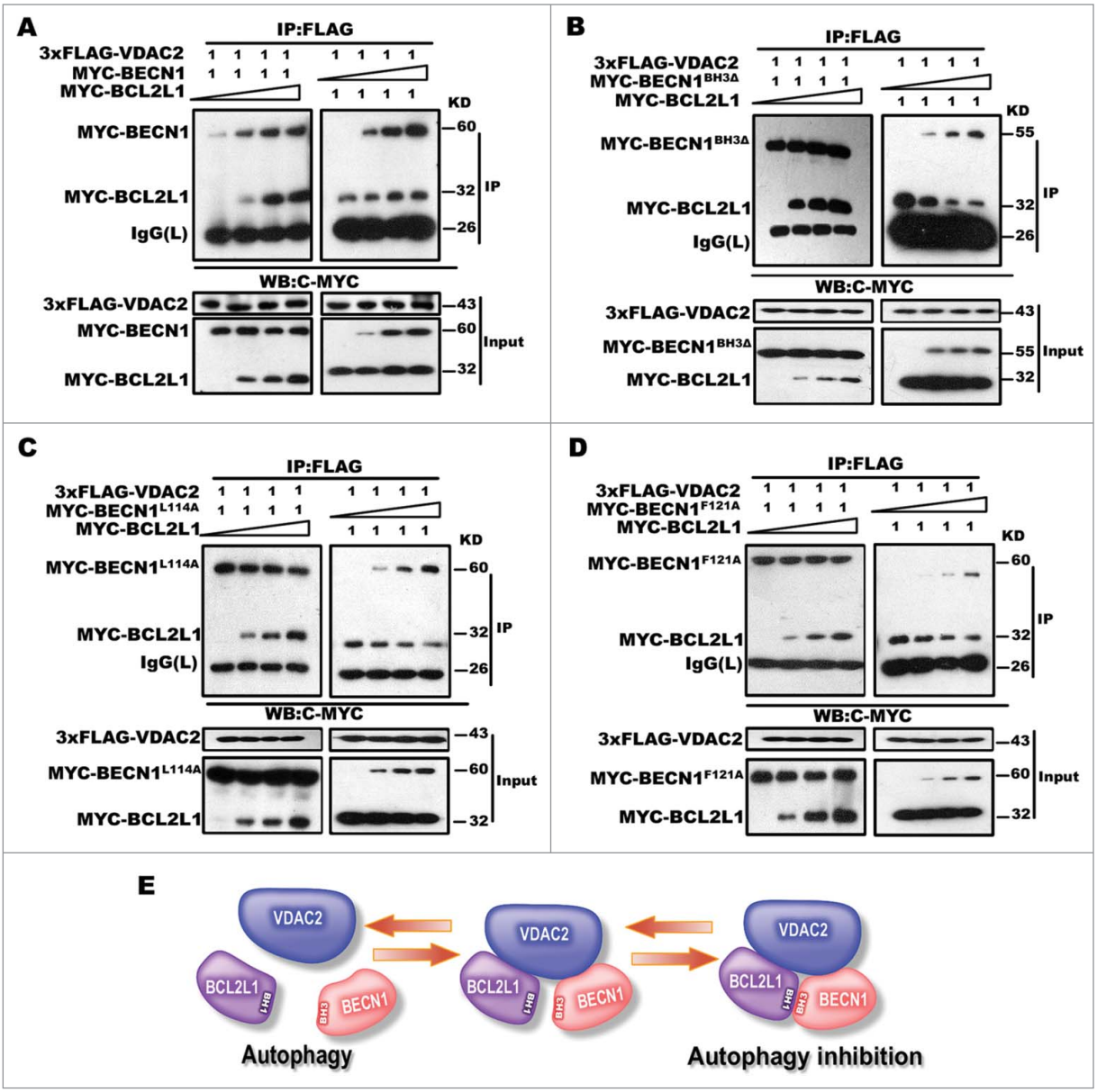

Figure 11. BECN1 or BCL2L1 promotes the VDAC2 interaction with BCL2L1 or with BECN1. (**A**) VDAC2 was cotransfected with pMyc-*Becn1* (1 μg) or pMyc-*Bcl2l1* (1 μg) and an increasing amount (0, 0.3, 0.6, and 1.2 μg) of pMyc-*Bcl2l1* (left panel) or pMyc-*Becn1* (right panel). The cell lysates were immunoprecipitated with the anti-FLAG antibody, followed by immunoblotting with the anti-MYC antibody. The whole cell lysates were examined by western blotting using the anti-MYC or anti-FLAG antibody (input). (**B**) MYC-BCL2L1 does not affect the VDAC2 interaction with the BECN1 BH3-deleted mutant, whereas the BECN1 BH3-deleted mutant inhibits the VDAC2 interaction with BCL2L1. VDAC2 was cotransfected with the BECN1 BH3-deleted mutant (pMyc-*Becn1*$^{BH3\Delta}$) (1 μg) or pMyc-*Bcl2l1* (1 μg) and an increasing amount (0, 0.3, 0.6, and 1.2 μg) of pMyc-*Bcl2l1* (left panel) or pMyc-*Becn1*$^{BH3\Delta}$ (right panel). (**C** and **D**) MYC-BCL2L1 does not affect the VDAC2 interaction with the BECN1 BH3, L114A (**C**), or F121A (**D**) point mutant, whereas the point mutants inhibit the VDAC2 interaction with BCL2L1. Transfection and coimmunoprecipitation were performed as in panel (**A**). (**E**) A model of VDAC2 inhibiting autophagy through stabilizing the interaction between BECN1 and BCL2L1. The free BECN1, which is a key autophagy initiation protein, initiates the formation of phagophores. When autophagy is inhibited, VDAC2 enhances the interaction between BECN1 and BCL2L1. When autophagy occurs, the VDAC2 interaction with BECN1 promotes the separation of BCL2L1 from the complex, then BECN1 dissociates from its interaction with VDAC2.

MYC-ATG5 and MYC-ATG16L1 constructs were the same as in our previous study.[32]

Antibodies and kits

The following primary antibodies were used: anti-VDAC2 (Abcam Inc., ab37985) for IF and western blot analysis, anti-VDAC2 (Proteintech Group, 11663-1-AP) for IP analysis, anti-ACTB (Proteintech Group, 20536-1-AP), anti-GATA1 (Abcam Inc., ab11963), anti-GATA2 (Abcam Inc., ab22849), anti-SP1 (Abcam Inc., ab13370), anti-MYBL2 (Santa Cruz Biotechnology, sc-725), anti-LC3B (Cell Signaling Technology, 3868s), anti-ATG16L1 (Cell Signaling Technology, 8089s), anti-

BECN1 (MBL, PD017), anti-FLAG (Sigma-Aldrich, F3165), anti-MYC/c-MYC (Roche Applied Science, 11667149001), anti-GFP (Roche Applied Science, 11814460001), anti-ATG5 (Abgent, AP1812b) and anti-CASP3 (ZSGB-BIO, PR-0284). TUNEL kit is from (Qihaifutai, AT005-2). The anti-ACTB, anti-ATG5, anti-ATG16L1, anti-CASP3, anti-LC3B, anti-MYBL2 and anti-VDAC2 antibodies can be used to detect same proteins from both pigs and mice.

The following secondary antibodies were used: peroxidase-conjugated AffiniPure goat anti-mouse IgG, light chain* specific (Jackson ImmunoResearch Laboratories, 115-035-174), peroxidase-conjugated AffiniPure F(ab′)2 fragment rabbit anti-mouse IgG, Fc fragment specific (Jackson ImmunoResearch Laboratories, 315-036-046), peroxidase-conjugated AffiniPure mouse anti-Rabbit IgG, light chain* specific (Jackson ImmunoResearch Laboratories, 211-032-171), peroxidase-conjugated AffiniPure F (ab′)2 fragment goat anti-Rabbit IgG, Fc fragment specific (Jackson ImmunoResearch Laboratories, 211-032-170), Dylight™ 594-conjugated secondary antibody (Jackson ImmunoResearch Laboratories, DkxRb-003-D594NHSX), goat anti-rabbit IgG horseradish peroxidase (HRP)-linked whole antibody (Pierce Company, SA1–9510), and AMCA-conjugated AffiniPuregoatanti-mouse IgG (H^+L) (Proteintech Group, SA00010–1).

Cell culture, transfection, and dual-luciferase reporter assays

vdac2$^{-/-}$ and wild-type MEF cells were provided by Dr. William J. Craigen of Baylor College of Medicine.[22] NIH-3T3, CHO, HeLa, and HEK293T cells were obtained from China Center for Type Culture Collection (CCTCC, 3115CNCB00230, 3115CNCB00631, 3115CNCB00209 and 3115CNCB00266). The cells were cultured in high glucose DMEM (Dulbecco's modified Eagle's medium) with 10% fetal bovine serum in 12- or 48-well plates. For transfection, Lipofectamine™ 2000 (2 μl) (Invitrogen, 11668027) was used in each well. For luciferase assays, each wt or deletion construct was transfected at 400 ng, together with 10 ng/well of pRL-TK (Promega, E2241). After transfection, luciferase activities were measured using a dual-luciferase reporter assay system (Promega) and a Modulus Single Tube Multimode Reader (Turner Biosystems, Sunnyvale, CA, USA). Experiments were independently repeated at least 3 times, and the results were expressed as the means ± SD.

Oocyte and granule cell isolation and bisulfite-PCR methylation analysis

The isolation of ovarian cells from Kunming mice was performed as follows: Briefly, mouse ovaries at 2 dpp were minced in axenic phosphate-buffered saline (PBS; 137 Mm NaCl, 1.4 Mm KH_2PO_4, 4.3 Mm Na_2HPO_4, 2.7 Mm KCl) and then displaced into IV collagenase (Sigma-Aldrich, C5138) in a 37°C water bath for 20 min with shaking. The cells were centrifuged at 3,000 g for 10 min to remove collagenase, resuspended in D-Hanks (Thermo, SH3003002) with 0.05% trypsin-EDTA, and then centrifuged at 3,000 g for 10 min to collect the cells. The cells were cultured in dishes coated with 0.1% gelatin (Wako, 190-15805) for 5 h. The unattached (oocytes) and the attached (stroma) cells were collected. The growing oocytes and granulosa cells were collected from ovarian follicles of 14-d-old mice using the methods described previously.[53] The oocytes and granulosa cells of adult mice were directly collected from the uterine tube, and hyaluronidase (0.1% w/v, Sigma, H3506) was used to separate oocytes and granulosa cells. For DNA methylation analysis, sodium bisulfite treatment of genomic DNA from these isolated cells was performed as described in a previous study.[54] The sequencing primers are described in **Table S1**.

Virus generation and infection

Lentiviral vectors were cotransfected with the lentiviral packaging vectors pRSV-Rev (Addgene, #12253), pMD2.G (Addgene, #12259) and pCMV-VSV-G (Addgene, #8454) into HEK293T cells using Lipofectamine™2000. The collected supernatants were filtered through a 0.45-μm filter after transfection for 48 h and used directly to infect MEF cells.

Chromatin immunoprecipitation (ChIP)

Mouse ovaries were cut into small pieces, and 1% formaldehyde-PBS was used for cross-linking for 15 min with constant shaking. Then, glycine was added to a final concentration of 0.125 M to terminate the formaldehyde crosslinking. The other steps were described in a previous study.[54] The supernatant fraction chromatin was immunoprecipitated with antibodies as indicated, with no antibody (beads only) and with preimmune IgG (Boster, AR1010) together with protein G PLUS-agarose (Santa Cruz Biotechnology, Sc-2002). DNA from the immunoprecipitated complex was PCR-amplified using primers flanking −506 to −230 bp of the *Vdac2* genomic sequence. As a control, a 165-bp region approximately 7 kb downstream of exon 7 of the *Vdac2* gene was amplified. The primer sequences are described in **Table S1**. The PCR fragments were cloned into the T-easy vector (Promega, A137A) and sequenced.

Electrophoretic mobility shift assays (EMSA)

Oligos corresponding to the GATA-like element, MBS1 and MBS2 of the *Vdac2* promoter were annealed into double strands. Their sequences are described in **Table S1**. EMSA was performed as described previously.[54] Briefly, the annealed oligos (250 ng) were incubated with 20 μCi [γ−^{32}P] dATP and T4 polynucleotide kinase (Promega, M180A) for 1 h at 37°C to generate the radiolabeled probes, which were subsequently used in a G-50 column (Amersham Biosciences, 27-5330-01) to separate from free nucleotides for purification.

Western blot analysis and coimmunoprecipitation assays

Western blot analysis was performed using routine protocols. Protein extracts (50 μg) from tissues and cell lines were separated in12% SDS-polyacrylamide gels and then transferred onto 0.45-μm membranes (Amersham Pharmacia Biotech, Hybond-P). The indicated primary antibodies were incubated with the membranes overnight at 4°C. The membranes were washed in TBST (20 mM Tris-HCl pH7.5, 150 mM NaCl, 0.1% Tween 20) several times, incubated with the indicated HRP-conjugated secondary antibody for 1 h at room temperature and then washed in

TBST several times. A Super Signal Chemiluminescent Substrate system (Pierce, Rockford, 34080) was used to detect the signals.

Coimmunoprecipitation was used to analyze protein interactions in vitro. 293T cells were cotransfected with related plasmid DNAs. After 48 h, the cells were lysed in NETN buffer (50 mM Tris-HCl at pH 8.0, 0.15 M NaCl, 1 mM EDTA, and 0.5% NP-40 [Biosharp, 74388]) containing protease inhibitor cocktail (Roche, 04693159001). The other steps are described in a previous study.[32]

Immunofluorescence analysis

Ovary tissues were embedded in OCT medium (Tissue-Tek, Miles, 4583) and cut into a series of 6-μm sections using a cryostat (Leica, Bensheim, Germany). MEF and HeLa cells were cultured on glass coverslides. Both sections and coverslides were fixed with precooling methanol for 20 min at −20°C and permeabilized with 1% Triton X-100 (Sigma, 9002-93-1) in PBS for 30 min. The other steps were described in a previous study.[54] Images were acquired by confocal fluorescence microscopy (FV1000, Olympus, Tokyo, Japan).

Real-time and semi-quantitative RT-PCR

TRIzol (Invitrogen, 15596-026) was used to isolate total RNA, which was transcribed using a poly $(T)_{18}$ primer and reverse transcriptase (Promega, M1701). Platinum SYBR Green qPCR Super Mix-UDG (Invitrogen, D01010A) was used for real-time PCR amplification of *Vdac2* in a StepOne real-time PCR system (Applied Biosystems). Total RNA was also isolated from adult pig ovaries, semiquantitative RT-PCR was used to amplify both Ss*ATG5 and* Ss*ATG16L1*. Ss*ACTB* mRNA was amplified as a control, and the primer sequences are described in **Table S1**.

Production of transgenic pigs

pTrans-Flag-Ss*VDAC2* DNA was digested with Bsplu11I and gel purified. This DNA was microinjected into the pronuclei of fertilized eggs from Landrace pigs, and the fertilized eggs were transferred into the oviduct of surrogates for development. Genomic DNA was isolated from ears. Southern blot analysis was performed using routine protocols. Hybridization was performed at 68°C in hybridization solution (6X SSC [0.9 M NaCl, 0.1M sodium citrate], 5X Denhart [0.1g PVP-40, 0.1g FICOLL400, 0.1 g BSA], 0.5% SDS [Biosharp, L0024], and 100 μg/ml denatured salmon sperm DNA [Invitrogen, 15632-011]) with [$\alpha-^{32}$P] dCTP-labeled probe (a BamHI-cut fragment from the transgenic vector, which contains a 750 bp sequence of Ss*VDAC2* CDS. PCR identification was performed using the primers described in **Table S1**.

Histological and TUNEL assays

Ovary tissues were embedded in OCT medium (Tissue-Tek, Miles, 4583) and frozen at −20°C, then cut into serial 7-μm sections with a crystal microtome (CM1850, Leica, Bensheim, Germany). The sections were stained by haematoxylin and eosin, and images were taken by a Leica microsystems (Leica, Bensheim, Germany). For TUNEL assays, the sections were incubated with the rTdT mix containing FITC-dUTP at 37°C for 1 h. The fragmented DNA of apoptotic cells by catalytically incorporating FITC-dUTP was detected directly by fluorescence microscopy. The nuclei were stained by propidium iodide.

Disclosure of Potential Conflicts of Interest

No potential conflicts of interest were disclosed.

Acknowledgments

Authors thank professor William J. Craigen of Baylor College of Medicine for providing *Vdac* KO cell lines, and Drs. Xinmin Zheng and Li Li of Institute of Animal Husbandry and Veterinary, Hubei Academy of Agricultural Sciences for transgenic pig production.

Funding

This work was supported by the National Natural Science Foundation of China, the National Key Basic Research project and the Key Transgenic New Organism Project.

Supplemental data

Supplemental data for this article can be accessed on the publisher's website.

References

1. Jiang ZZ, Hu MW, Wang ZB, Huang L, Lin F, Qi ST, Ouyang YC, Fan HY, Schatten H, Mak TW, et al. Survivin is essential for fertile egg production and female fertility in mice. Cell Death Dis 2014; 5:e1154; PMID:24675472; http://dx.doi.org/10.1038/cddis.2014.126
2. Choi J, Jo M, Lee E, Choi D. AKT is involved in granulosa cell autophagy regulation via mTOR signaling during rat follicular development and atresia. Reproduction 2014; 147:73-80; PMID:24131573; http://dx.doi.org/10.1530/REP-13-0386
3. Zhang M, Su YQ, Sugiura K, Xia G, Eppig JJ. Granulosa cell ligand NPPC and its receptor NPR2 maintain meiotic arrest in mouse oocytes. Science 2010; 330:366-9; PMID:20947764; http://dx.doi.org/10.1126/science.1193573
4. Matsuda F, Inoue N, Manabe N, Ohkura S. Follicular growth and atresia in mammalian ovaries: regulation by survival and death of granulosa cells. J Reprod Dev 2012; 58:44-50; PMID:22450284; http://dx.doi.org/10.1262/jrd.2011-012
5. Su YQ, Sugiura K, Eppig JJ. Mouse oocyte control of granulosa cell development and function: paracrine regulation of cumulus cell metabolism. Semin Reprod Med 2009; 27:32-42; PMID:19197803; http://dx.doi.org/10.1055/s-0028-1108008
6. Inoue N, Matsuda F, Goto Y, Manabe N. Role of cell-death ligand-receptor system of granulosa cells in selective follicular atresia in porcine ovary. J Reprod Dev 2011; 57:169-75; PMID:21551974; http://dx.doi.org/10.1262/jrd.10-198E
7. Su YQ, Wu X, O'Brien MJ, Pendola FL, Denegre JN, Matzuk MM, Eppig JJ. Synergistic roles of BMP15 and GDF9 in the development and function of the oocyte-cumulus cell complex in mice: genetic evidence for an oocyte-granulosa cell regulatory loop. Dev Biol 2004; 276:64-73; PMID:15531364; http://dx.doi.org/10.1016/j.ydbio.2004.08.020
8. Ratts VS, Flaws JA, Kolp R, Sorenson CM, Tilly JL. Ablation of bcl-2 gene expression decreases the numbers of oocytes and primordial follicles established in the post-natal female mouse gonad. Endocrinology 1995; 136:3665-8; PMID:7628407
9. Hsu SY, Lai RJ, Finegold M, Hsueh AJ. Targeted overexpression of Bcl-2 in ovaries of transgenic mice leads to decreased follicle apoptosis, enhanced folliculogenesis, and increased germ cell tumorigenesis. Endocrinology 1996; 137:4837-43; PMID:8895354
10. Perez GI, Robles R, Knudson CM, Flaws JA, Korsmeyer SJ, Tilly JL. Prolongation of ovarian lifespan into advanced chronological age by Bax-deficiency. Nat Genet 1999; 21:200-3; PMID:9988273; http://dx.doi.org/10.1038/5985
11. Basavarajappa MS, Karman BN, Wang W, Gupta RK, Flaws JA. Methoxychlor induces atresia by altering

Bcl2 factors and inducing caspase activity in mouse ovarian antral follicles in vitro. Reprod Toxicol 2012; 34:545-51; PMID:23000595; http://dx.doi.org/10.1016/j.reprotox.2012.08.007
12. Tanner EA, Blute TA, Brachmann CB, McCall K. Bcl-2 proteins and autophagy regulate mitochondrial dynamics during programmed cell death in the Drosophila ovary. Development 2011; 138:327-38; PMID:21177345; http://dx.doi.org/10.1242/dev.057943
13. Maiuri MC, Le Toumelin G, Criollo A, Rain JC, Gautier F, Juin P, Tasdemir E, Pierron G, Troulinaki K, Tavernarakis N, et al. Functional and physical interaction between Bcl-X(L) and a BH3-like domain in Beclin-1. EMBO J 2007; 26:2527-39; PMID:17446862; http://dx.doi.org/10.1038/sj.emboj.7601689
14. Pattingre S, Tassa A, Qu X, Garuti R, Liang XH, Mizushima N, Packer M, Schneider MD, Levine B. Bcl-2 antiapoptotic proteins inhibit Beclin 1-dependent autophagy. Cell 2005; 122:927-39; PMID:16179260; http://dx.doi.org/10.1016/j.cell.2005.07.002
15. Hou YC, Chittaranjan S, Barbosa SG, McCall K, Gorski SM. Effector caspase Dcp-1 and IAP protein Bruce regulate starvation-induced autophagy during Drosophila melanogaster oogenesis. J Cell Biol 2008; 182:1127-39; PMID:18794330; http://dx.doi.org/10.1083/jcb.200712091
16. Nezis IP, Lamark T, Velentzas AD, Rusten TE, Bjorkoy G, Johansen T, Papassideri IS, Stravopodis DJ, Margaritis LH, Stenmark H, et al. Cell death during Drosophila melanogaster early oogenesis is mediated through autophagy. Autophagy 2009; 5:298-302; PMID:19066465; http://dx.doi.org/10.4161/auto.5.3.7454
17. Drummond-Barbosa D, Spradling AC. Stem cells and their progeny respond to nutritional changes during Drosophila oogenesis. Dev Biol 2001; 231:265-78; PMID:11180967; http://dx.doi.org/10.1006/dbio.2000.0135
18. Barth JM, Hafen E, Kohler K. The lack of autophagy triggers precocious activation of Notch signaling during Drosophila oogenesis. BMC Dev Biol 2012; 12:35; PMID:23217079; http://dx.doi.org/10.1186/1471-213X-12-35
19. Escobar ML, Echeverria OM, Ortiz R, Vazquez-Nin GH. Combined apoptosis and autophagy, the process that eliminates the oocytes of atretic follicles in immature rats. Apoptosis 2008; 13:1253-66; PMID:18690537; http://dx.doi.org/10.1007/s10495-008-0248-z
20. Choi JY, Jo MW, Lee EY, Yoon BK, Choi DS. The role of autophagy in follicular development and atresia in rat granulosa cells. Fertil Steril 2010; 93:2532-7; PMID:20149359; http://dx.doi.org/10.1016/j.fertnstert.2009.11.021
21. Gannon AM, Stampfli MR, Foster WG. Cigarette smoke exposure elicits increased autophagy and dysregulation of mitochondrial dynamics in murine granulosa cells. Biol Reprod 2013; 88:63; PMID:23325812; http://dx.doi.org/10.1095/biolreprod.112.106617
22. Cheng EH, Sheiko TV, Fisher JK, Craigen WJ, Korsmeyer SJ. VDAC2 inhibits BAK activation and mitochondrial apoptosis. Science 2003; 301:513-7; PMID:12881569; http://dx.doi.org/10.1126/science.1083995
23. Lazarou M, Stojanovski D, Frazier AE, Kotevski A, Dewson G, Craigen WJ, Kluck RM, Vaux DL, Ryan MT. Inhibition of Bak activation by VDAC2 is dependent on the Bak transmembrane anchor. J Biol Chem 2010; 285:36876-83; PMID:20851889; http://dx.doi.org/10.1074/jbc.M110.159301
24. Plotz M, Gillissen B, Hossini AM, Daniel PT, Eberle J. Disruption of the VDAC2-Bak interaction by Bcl-x(S) mediates efficient induction of apoptosis in melanoma cells. Cell Death Differ 2012; 19:1928-38; PMID:22705850; http://dx.doi.org/10.1038/cdd.2012.71
25. Ren D, Kim H, Tu HC, Westergard TD, Fisher JK, Rubens JA, Korsmeyer SJ, Hsieh JJ, Cheng EH. The VDAC2-BAK rheostat controls thymocyte survival. Sci Signal 2009; 2:ra48; PMID:19706873; http://dx.doi.org/10.1126/scisignal.2000274
26. Roy SS, Ehrlich AM, Craigen WJ, Hajnoczky G. VDAC2 is required for truncated BID-induced mitochondrial apoptosis by recruiting BAK to the mitochondria. EMBO Rep 2009; 10:1341-7; PMID:19820692; http://dx.doi.org/10.1038/embor.2009.219
27. Sarioglu H, Brandner S, Haberger M, Jacobsen C, Lichtmannegger J, Wormke M, Andrae U. Analysis of 2,3,7,8-tetrachlorodibenzo-p-dioxin-induced proteome changes in 5L rat hepatoma cells reveals novel targets of dioxin action including the mitochondrial apoptosis regulator VDAC2. Mol Cell Proteomics 2008; 7:394-410; PMID:17998243; http://dx.doi.org/10.1074/mcp.M700258-MCP200
28. Sampson MJ, Decker WK, Beaudet AL, Ruitenbeek W, Armstrong D, Hicks MJ, Craigen WJ. Immotile sperm and infertility in mice lacking mitochondrial voltage-dependent anion channel type 3. J Biol Chem 2001; 276:39206-12; PMID:11507092; http://dx.doi.org/10.1074/jbc.M104724200
29. Huang H, Hu X, Eno CO, Zhao G, Li C, White C. An interaction between Bcl-xL and the voltage-dependent anion channel (VDAC) promotes mitochondrial Ca2+ uptake. J Biol Chem 2013; 288:19870-81; PMID:23720737; http://dx.doi.org/10.1074/jbc.M112.448290
30. Shimizu S, Narita M, Tsujimoto Y. Bcl-2 family proteins regulate the release of apoptogenic cytochrome c by the mitochondrial channel VDAC. Nature 1999; 399:483-7; PMID:10365962; http://dx.doi.org/10.1038/20959
31. Geisler S, Holmstrom KM, Skujat D, Fiesel FC, Rothfuss OC, Kahle PJ, Springer W. PINK1/Parkin-mediated mitophagy is dependent on VDAC1 and p62/SQSTM1. Nat Cell Biol 2010; 12:119-31; PMID:20098416; http://dx.doi.org/10.1038/ncb2012
32. Chen. K, Huang. C, Yuan. J, Cheng. H, Zhou R. Long-term artificial selection reveals a role of TCTP in autophagy in mammalian cells. Mol Biol Evol 2014; 31:2194-211; http://dx.doi.org/10.1093/molbev/msu181; PMID:24890374
33. Peng X, Sun H, Mei S, Li L, Song Z, Wu H. The breeding progress of hubei white high grade line. Hubei Agr Sci 2010; 49 3120-2
34. See MT, Mabry JW, Bertrand JK. Restricted maximum likelihood estimation of variance components from field data for number of pigs born alive. J Anim Sci 1993; 71:2905-9; PMID:8270513
35. Liang XH, Kleeman LK, Jiang HH, Gordon G, Goldman JE, Berry G, Herman B, Levine B. Protection against fatal Sindbis virus encephalitis by beclin, a novel Bcl-2-interacting protein. J Virol 1998; 72:8586-96; PMID:9765397
36. Johnson J, Canning J, Kaneko T, Pru JK, Tilly JL. Germline stem cells and follicular renewal in the postnatal mammalian ovary. Nature 2004; 428:145-50; PMID:15014492; http://dx.doi.org/10.1038/nature02316
37. Zou K, Yuan Z, Yang Z, Luo H, Sun K, Zhou L, Xiang J, Shi L, Yu Q, Zhang Y, et al. Production of offspring from a germline stem cell line derived from neonatal ovaries. Nat Cell Biol 2009; 11:631-6; PMID:19363485; http://dx.doi.org/10.1038/ncb1869
38. Peters H. The development of the mouse ovary from birth to maturity. Acta Endocrinol (Copenh) 1969; 62:98-116; PMID:5394354
39. Zielak AE, Forde N, Park SD, Doohan F, Coussens PM, Smith GW, Ireland JJ, Lonergan P, Evans AC. Identification of novel genes associated with dominant follicle development in cattle. Reprod Fertil Dev 2007; 19:967-75; PMID:18076829; http://dx.doi.org/10.1071/RD07102
40. Kuma A, Hatano M, Matsui M, Yamamoto A, Nakaya H, Yoshimori T, Ohsumi Y, Tokuhisa T, Mizushima N. The role of autophagy during the early neonatal starvation period. Nature 2004; 432:1032-6; PMID:15525940; http://dx.doi.org/10.1038/nature03029
41. Tsukamoto S, Kuma A, Murakami M, Kishi C, Yamamoto A, Mizushima N. Autophagy is essential for preimplantation development of mouse embryos. Science 2008; 321:117-20; PMID:18599786; http://dx.doi.org/10.1126/science.1154822
42. Gawriluk TR, Hale AN, Flaws JA, Dillon CP, Green DR, Rucker EB 3rd. Autophagy is a cell survival program for female germ cells in the murine ovary. Reproduction 2011; 141:759-65; PMID:21464117; http://dx.doi.org/10.1530/REP-10-0489
43. Tilly JL, Tilly KI, Kenton ML, Johnson AL. Expression of members of the bcl-2 gene family in the immature rat ovary: equine chorionic gonadotropin-mediated inhibition of granulosa cell apoptosis is associated with decreased bax and constitutive bcl-2 and bcl-xlong messenger ribonucleic acid levels. Endocrinology 1995; 136:232-41; PMID:7828536
44. Johnson AL, Bridgham JT, Jensen T. Bcl-X(LONG) protein expression and phosphorylation in granulosa cells. Endocrinology 1999; 140:4521-9; PMID:10499507
45. Wirawan E, Lippens S, Vanden Berghe T, Romagnoli A, Fimia GM, Piacentini M, Vandenabeele P. Beclin1: a role in membrane dynamics and beyond. Autophagy 2012; 8:6-17; PMID:22170155; http://dx.doi.org/10.4161/auto.8.1.16645
46. Kang R, Zeh HJ, Lotze MT, Tang D. The Beclin 1 network regulates autophagy and apoptosis. Cell Death Differ 2011; 18:571-80; PMID:21311563; http://dx.doi.org/10.1038/cdd.2010.191
47. Liang XH, Jackson S, Seaman M, Brown K, Kempkes B, Hibshoosh H, Levine B. Induction of autophagy and inhibition of tumorigenesis by beclin 1. Nature 1999; 402:672-6; PMID:10604474; http://dx.doi.org/10.1038/45257
48. Yue Z, Jin S, Yang C, Levine AJ, Heintz N. Beclin 1, an autophagy gene essential for early embryonic development, is a haploinsufficient tumor suppressor. Proc Natl Acad Sci U S A 2003; 100:15077-82; PMID:14657337; http://dx.doi.org/10.1073/pnas.2436255100
49. Qu X, Yu J, Bhagat G, Furuya N, Hibshoosh H, Troxel A, Rosen J, Eskelinen EL, Mizushima N, Ohsumi Y. et al. Promotion of tumorigenesis by heterozygous disruption of the beclin 1 autophagy gene. J Clin Invest 2003; 112:1809-20; PMID:14638851; http://dx.doi.org/10.1172/JCI20039
50. Oberstein A, Jeffrey PD, Shi Y. Crystal structure of the Bcl-XL-Beclin 1 peptide complex: Beclin 1 is a novel BH3-only protein. J Biol Chem 2007; 282:13123-32; PMID:17337444; http://dx.doi.org/10.1074/jbc.M700492200
51. Gurkar AU, Chu K, Raj L, Bouley R, Lee SH, Kim YB, Dunn SE, Mandinova A, Lee SW. Identification of ROCK1 kinase as a critical regulator of Beclin1-mediated autophagy during metabolic stress. Nat Commun 2013; 4:2189; PMID:23877263; http://dx.doi.org/10.1038/ncomms3189
52. Zalckvar E, Berissi H, Mizrachy L, Idelchuk Y, Koren I, Eisenstein M, Sabanay H, Pinkas-Kramarski R, Kimchi A. DAP-kinase-mediated phosphorylation on the BH3 domain of beclin 1 promotes dissociation of beclin 1 from Bcl-XL and induction of autophagy. EMBO Rep 2009; 10:285-92; PMID:19180116; http://dx.doi.org/10.1038/embor.2008.246
53. Hiura H, Obata Y, Komiyama J, Shirai M, Kono T. Oocyte growth-dependent progression of maternal imprinting in mice. Genes Cells 2006; 11:353-61; PMID:16611239; http://dx.doi.org/10.1111/j.1365-2443.2006.00943.x
54. Hou Y, Yuan J, Zhou X, Fu X, Cheng H, Zhou R. DNA demethylation and USF regulate the meiosis-specific expression of the mouse Miwi. PLoS Genet 2012; 8:e1002716; PMID:22661915; http://dx.doi.org/10.1371/journal.pgen.1002716